Egypt. J. Chem. **Vol.**:68, No.:5, pp.:673– 697 (2025)

Egyptian Journal of Chemistry

http://ejchem.journals.ekb.eg/

Nano Polyethylene terephthalate (PET) electrospun fiber from plastic waste for heavy metals removal from wastewater

Ghada A. Amin [1], Ghada A. Kadry [2], Taha M.A. Razek [1], and Ahmed G. Hassabo [3] *

[1] *Department of Environmental Basic Science, Faculty of Environmental Studies and Research, Ain Shams University,Cairo, Egypt*

[2] *Chemical Engineering Department, National Research Centre Higher Institute of Engineering, El-Shorouk Academy. Cairo, Egypt*

[3] *National Research Centre (NRC, Scopus affiliation ID 60014618), Textile Research and Technology Institute (TRTI), Pre-treatment and Finishing of Cellulose-based Fibers Department (PFCFD), El-Behouth St. (former El-Tahrir str.), Dokki, P.O. 12622, Giza, Egypt*

Abstract

One of the greatest inventions of the twenty-first century, plastics benefit humans in many facets of life, including construction, healthcare, packaging, agriculture, and automobiles. The production of plastic is growing quickly due to rising demand and ease of processing, which is causing a significant amount of garbage to accumulate in the environment. Plastic waste management is an open challenge and a threat to the global environment due to several factors, including a lack of infrastructure, poorly managed recycling facilities and technologies, ineffective waste collection systems, improper and unrestrained disposal practices, and a lack of awareness. Incineration, landfilling, recycling, and reuse were once thought to be the most effective methods for managing plastic garbage, but they were deemed insufficient to address the problem's significant magnitude, and all these methods were considered to conflict with SDG sustainable developed goals. Additionally, plastic waste (PW) can cause cancer, harm to the neurological system, fast genetic changes, and metabolic issues in people because of its chemical makeup and long disintegration times. This article examines plastic waste recycling, focusing on polyethylene terephthalate (PET) recycling through electrospinning to produce nanofiber membranes. The study investigates the effects of different solvent systems and chitosan addition on PET nanofiber morphology and properties. Electrospinning parameters were optimized, and the resulting nanofibers were characterized using scanning electron microscopy. The nanofiber membranes were also evaluated for metal ion adsorption capacity. Results indicate that a TFA/DCM (70:30) solvent mixture produced the most uniform PET nanofibers, with fiber diameter decreasing upon chitosan addition. The PET/chitosan nanofiber membranes demonstrated promising moisture management and metal ion adsorption properties, suggesting potential applications in water purification and filtration. This research contributes to addressing plastic waste management challenges while developing value-added products from recycled materials.

Keywords: Electrospinning, PET electrospinning, nanofiber membranes, heavy metal adsorption, chitosan, moisture management

1. Introduction

Nano Polyethylene terephthalate (PET) electrospun fibers derived from plastic waste have emerged as a promising solution for heavy metal removal from wastewater. This innovative approach addresses two critical environmental challenges simultaneously: the management of plastic waste and the treatment of contaminated water sources.

Environmental pollution is a growing global concern, affecting public health, ecosystems, and climate stability. Various pollutants contribute to serious health risks, including respiratory diseases, cardiovascular conditions, and developmental disorders. In many developing countries, ineffective waste management systems and limited technological advancements exacerbate pollution-related challenges. Among the major sources of environmental pollution, plastic waste remains one of the most persistent and problematic materials.[1-13]

Polyethylene terephthalate (PET), a commonly used plastic in packaging-especially in disposable water bottles-poses a significant environmental threat due to its resistance to natural degradation.[14] Conventional disposal methods, such as landfilling and incineration, are not sustainable solutions as they contribute to soil and air pollution. Recycling PET waste into valuable materials offers a more sustainable and eco-friendly alternative, helping to reduce plastic accumulation while creating useful products.[15]Electrospinning is a widely recognized technique for fabricating nanofiber membranes with high surface area and interconnected porosity.

These properties make electrospun PET fibers highly effective for applications such as filtration, pollutant removal, and textile development. The incorporation of additives like chitosan can further enhance the adsorption capacity and functional properties of PET nanofibers, making them more efficient in environmental applications.[16]

* Corresponding author: aga.hassabo@hotmail.com

Received date 16 February 2025; Revised date 14 March 2025; Accepted date 27 March 2025

DOI: 10.21608/ejchem.2025.360942.11311

Often used thermoplastic polymer, PET is employed in packaging materials and single-use plastic goods. Because of its non-biodegradable character and long-lasting environmental impact, the accumulation of PET waste in landfills and oceans has grown worldwide a cause of worry. Researchers have discovered a means to reduce plastic pollution and generate value-added goods for environmental restoration by reusing PET trash into useful nanomaterials. A flexible method called electrospinning lets one create ultra-fine fibers with sizes varying from nanometers to micrometers. Applied to PET waste, this method produces nanofibers with high surface area-to-volume ratios, improved mechanical qualities, and distinctive surface features. These attributes make nano PET electrospun fibers especially fit for adsorption uses, including heavy metal removal from wastewater.

Severe hazards to human health and ecosystems arise from heavy metal poisoning of water supplies. Low-concentration heavy metal removal from conventional water treatment systems is sometimes challenging. High adsorption capacity, selectivity, and re-generation potential of nano PET electrospun fibers provide a possible answer. Utilizing ion exchange, surface complexation, and physical adsorption, the nanoscale size and surface changes of these fibers enable the effective capture of heavy metal ions through several channels.

Examining the production, characterization, and use of micro PET electrospun fibers in heavy metal removal from wastewater will be put up in this introduction. In line with world efforts toward circular economy and environmental preservation, the research in this subject not only helps to advance water treatment technology but also supports sustainable practices in plastic waste management.

This study explores the production and characterization of PET-based electro-spun nanofibers derived from recycled plastic waste. The research investigates how different solvent combinations and the addition of chitosan affect fiber morphology and adsorption efficiency. The resulting nanofiber membranes are evaluated for their ability to remove heavy metals from wastewater, offering a sustainable approach to both plastic waste management and water purification.

2. Experimental

2.1. Materials

Polyethylene terephthalate (PET) from water packing local water-packing company produced as waste materials. Chitosan, medium molecular weight, Brookfield viscosity 80,000 cps, tetrabutyl ammonium bromide (TBAB; $(CH_3CH_2CH_2CH_2)\ N^+Br^-$), were purchased from Sigma Aldrich Co. for Chemical (Germany). Trifluoroacetic acid (TFA; CF_3COOH, 98%), and Dichloromethane (DCM; CH_2Cl_2; 99.5%) were purchased from Loba Co. for Chemical (India). Cobalt nitrate ($Co(NO_3)_2$), nickel nitrate ($Ni(NO_3)_2$),Manganese nitrate Mn(NO3)2,and copper nitrate ($Cu(NO_3)_2$) were purchased from Loba Co. for Chemical (India)as an analytical grade.

2.2. Methods

2.2.1. Preparation of polymer solution for electrospinning

Recycled polyethylene terephthalate (PET) was obtained from water bottles (1.5 L) collected from the same production batch (Egyptian local market). The molecular weight of this type of PET, commonly used during PET bottle production, typically lies in the range of 30–80 kDa. [17] All the bottles were cleaned by removing the non-PET components such as labels and rinsed with pure ethanol before drying, followed by shredding into small pieces $5 \times 5\ mm^2$.

The recycled PET was added to a different solvent mixture (TFA/DCM (100:0, 50:50, 70: 30, and 0: 100) at concentrations of 15 wt%. Solutions were mixed for 24 h to ensure complete dissolution of the PET at a temperature of 20°C. After that, chitosan was mixed with PET in a selective solvent (15 %) by three different weights, 1, 2, and 3 %, and then applied to the electrospinning process using suitable conditions. All polymer solutions were mixed by using a magnetic stirrer for a sufficient time until they became homogeneous (24 h). The viscosity and electrical conductivity were measured by a digital viscometer and an electric conductivity meter (Adwa Co., GA, USA) at 25°C.

2.2.2. Electrospinning of PET

The PET solutions were electrospun by using a commercially available electrospinning setup. Syringe glass 10 ml filled with prepared solutions and connected with the positive part of electrospinning; the negative part connected to the rotated collector.

The electrospinning parameters were adjusted as follows: the syringe pump worked at a speed rate of 6 ml/h, at 25 KV, and 15 cm distance from the cathode. The prepared electro-spun fibers were collected for the characterization. [22] After that chitosan was mixed with PET solution (15 %) by three different weight percentages 1, 2, and 3 %, and then applied to the electrospinning process by the previous condition.

2.3. Analysis and measurements

2.3.1. Scanning Electron Microscopy

The morphology of both the electrospun PET and Pet/chitosan nanofiber mats were examined using a scanning electron microscope (SEM; Jeol, JSM 6010LV, Peabody, MA, USA). Every specimen was coated with a thin layer of gold.

2.3.2. Moisture measurement

The fabricated membrane was assessed for moisture management utilizing a moisture management tester (MMT) (model: M290, manufacturer: SDL Atlas, origin: UK) following the AATCC 195-2017. [18] The absorption rate, wetting time, spreading velocity, and maximum wetted radius of both the interior and exterior surfaces of the membrane, for classifying the membrane's interaction with liquids.

2.3.3. Adsorption and Isothermal Studies

To convert the measured absorbance into concentration and assess the adsorption of each metal salts (cobalt nitrate ($Co(NO_3)_2$), nickel nitrate ($Ni(NO_3)_2$), and copper nitrate ($Cu(NO_3)_2$) Manganese nitrate Mn(NO3)2 five known concentrations for each metal salts were prepared and analyzed using 5 cm quartz cells in a UV/visible spectrophotometer (UV-1601 Shimadzu, Japan). The calibration standard curve was created as depicted in **Figure 1**.

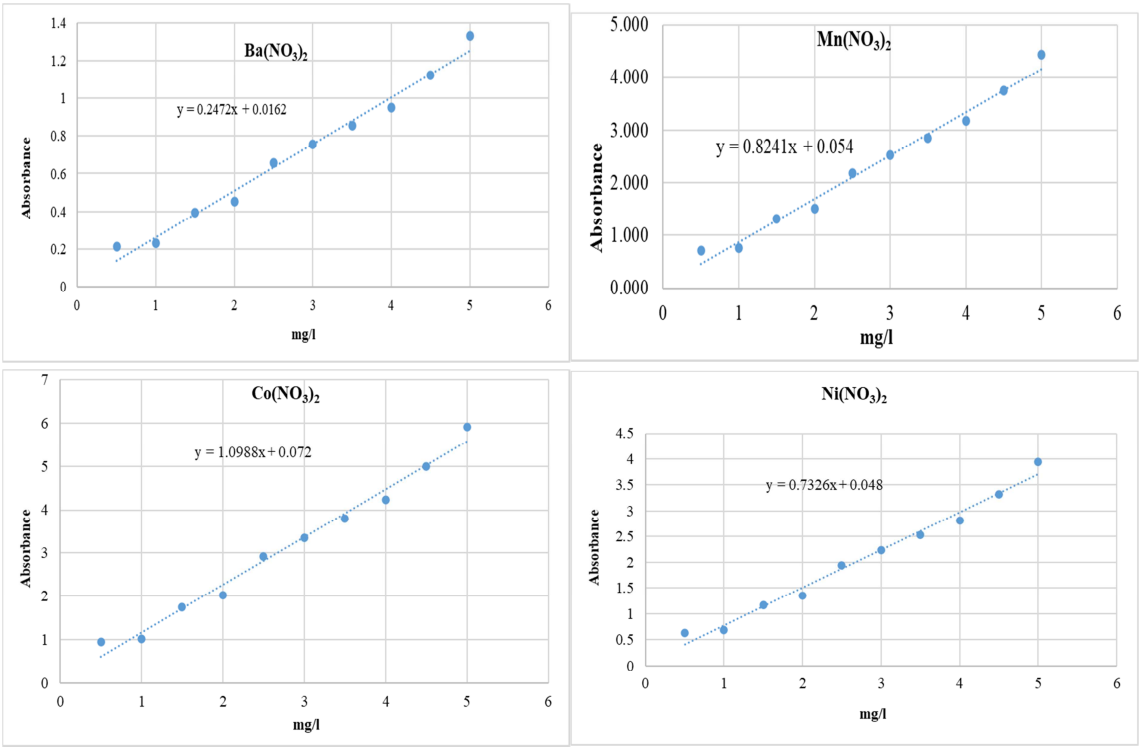

Figure 1: calibration standard curve for different metal salts

The batch adsorption studies were conducted in Erlenmeyer flasks that contained 100 ml of the metal salts solution with a concentration of 10-300 mg/L.

2 g of the natural network nanofibre was further added to the samples. The flasks were shaken on a horizontal shaker at a constant speed of 400 rpm and a temperature of 30°C. Subsequently, equilibrium was achieved by stirring the Erlenmeyer flasks for three hours. The UV/visible spectrophotometer (UV-1601 Shimadzu, Japan) was employed to detect the concentration of metal salts in the solution following equilibrium adsorption. All adsorption experiments were conducted in duplicate, and the mean values were reported.

For kinetic experiments, after the treatment, sampling was done at varied times (10–120 min). 5 ml of the sampled aqueous phase was tested for the residual concentration of metal salts using a UV-Vis spectrophotometer and then added back into the treatment solution to keep the concentration constant.

For isotherm investigations, 100 ml of the solutions of varied metal salt concentrations (10 – 300 mg/L) were produced in separate 250 ml conical flasks. 2g of nanofibre was placed into each of the conical flasks. After 30 min, the solution was tested then the absorbance was converted to concentration. Duplicate tests were done in parallel to check the results.

2.3.4. Analysis of errors

Due to the inherent predisposition resulting from the linearization of isotherm and dynamic models, four distinct error functions of the non-linear regression model were employed as criteria for assessing the quality of fit. [19-21]

2.3.4.1. The root mean square error (RMSE)

The root mean square error (RMSE) test has been employed by numerous analysts to evaluate the adequacy and accuracy of the model fit with the exploratory data.

$$\mathrm{RMSE} = \sqrt{\frac{1}{n-2}\sum_{i=1}^{n}(q_i - q_{i.e})^2}$$

Where q_i represents the test sorption limit from batch analysis I, $q_{i.e}$denotes the sorption capacity assessed from the sorption model to compare qi, and n signifies the number of observations in the batch experiment.

2.3.4.2. The chi-squared test (χ^2)

The chi-squared test (X^2) statistic is the aggregate of the squares of the discrepancies between the experimental data derived from evaluations of models, with each squared discrepancy divided by the corresponding data calculated from models. The chi-squared test exhibits some similarity to the root mean square error and is expressed as:

$$X^2 = \sum_{i=1}^{n} \frac{(q_i - q_{i.e})^2}{q_{i.e}}$$

2.3.4.3. The aggregate of absolute errors (AAE)

The sum of total errors (SAE) is expressed as:

$$\mathrm{SAE} = \sum_{i=1}^{n} |q_i - q_{i.e}|_i$$

The isotherm parameters regulated by this method yield an improved fit as the magnitude of the errors increases, skewing the fit towards the high-concentration data.

2.3.4.4. The mean relative error (MRE)

The average relative error (ARE) is defined as:

$$\mathrm{ARE} = \frac{100}{n} \sum_{i=1}^{n} \left| \frac{q_t - q_{i.e}}{q_t} \right|$$

This error function aims to restrict the fractional error distribution across the entire concentration range.

3. Result and Discussion

Ultrafine fibers may be produced from polymer solutions using electrospinning. [22-26] This approach may effectively generate fibers with sizes in the micrometer range of nanometers. The electrospinning process for fiber creation from polymer solutions is greatly affected by the solution's parameters, such as viscosity, surface tension, and net charge density.

Viscosities of 1 to 20 poise and surface tensions of 35 to 55 dynes/cm were suitable for fiber production in the electrospinning of PET solutions. Electrospinning was hindered at viscosities beyond 20 poise due to flow instability caused by the solution's elevated cohesiveness. Comprehending solvent systems is essential for controlling solution characteristics in the electrospinning process to generate ultrafine fibers.

Electrospun fibers may be designed to form diverse forms by utilizing solvents with high vapor pressure or by deliberately adding salt to the polymer solution, which is later removed after the fibers are dried. The resulting structure of electrospun fibers has a high surface-to-volume ratio, making them ideal for filtration, odor absorption, and many other smart textile applications. [27-29]

3.1. Characterization of manufactured nanofibers

The ideal parameters for spinning PET waste with solvents (trifluoracetic acid, dichloromethane, TFA/DCM (100:0, 50:50, 70:30, and 0:100)) included a flow rate of 6 mL/hr, a nozzle-holder distance of 10 cm, and an applied voltage of 20 kV, to investigate the effect of the solvents on fiber morphology. The viscosity, conductivity, and surface tension properties of the cellulose isolated from rice straw waste solutions were studied and are reported in

Table 1. Modifying the solvent led to changes in the properties of the polymer solution, such as conductivity and surface tension. This may enhance the polarity of the extracted cellulose solution.

Figure 2 shows the result of changing the solvent ratio (TFA/DCM (100:0, 50:50, 70: 30, and 0: 100) at concentrations of 15 wt%. of PET in the solvent. The average fiber diameter could be precisely controlled, while the fiber morphologies were almost unaffected and showed continuous long fibers with smooth surfaces.

The insets in the micrographs illustrate the size distribution of the fibers, derived from measuring the diameters of a minimum of 200 fibers for each sample. The mean fiber diameters were 2.5±0.26, 1±0.84, 1.4±0.63, and 2.3±0.63 μm for PET (15%) in TFA/DCM (100:0, 50:50, 70:30, and 0:100) respectively. The relative standard deviation was greatest for the thinner fibers and diminished with increasing fiber thickness, likely attributable to the lower viscosity and elevated surface tension of the electrospun solutions for these samples.

Figure 3 shows the relationship between the fiber diameter and different solvents. A mixture solvent of TFA and DCM had only a marginal effect on the thickness of the fibers. For all the evaluated formulations, the fibers with the greatest uniformity were always prepared at PET 15 wt % in TFA/DCM (70:30).

Figure 2 illustrates SEM pictures of PET electrospun fibers. The electrospinning of PET derived from each solvent yielded a wide and homogenous spun sheet. The uniformity was attributed to a completely soluble solution and consistent distribution caused by the steady effect of the electric field on the spun solution from the needle to the collector. Furthermore, utilizing TFA and DCM as a solvent produced a compact, centrally positioned bundle sheet. Figure 2 demonstrates that the thick fibers, arising from phase separation, were generated using TFA followed by DCM, whereas the use of TFA/DCM mixture as a solvent resulted in thinner fiber diameters.

This experiment concludes that utilizing TFA/DCM (70:30) as a solvent results in nanofibers with a lower diameter and a more homogeneously dispersed fiber. Consequently, additional research was conducted to examine the impact of mixing chitosan with PET utilizing TFA/DCM (70:30) as a solvent on the properties of the resulting nanofiber. The surface morphology of the electrospun fibers was routinely analyzed by SEM, as depicted in **Figure 2**. Modifying the solvent in the spinning of PET produced significant results. The TFA/DCM (70:30) solvent exhibited an efficient spinning process, yielding thinner fibers. SEM results demonstrated that morphology and fiber uniformity enhanced when the chitosan polymer concentration increased from 1 to 3%. Spinning at a low chitosan concentration (1%) resulted in uniform cylin-

drical fibers with a diameter of 1.5 ± 0.07 µm. The fiber diameter is almost stable by increasing the chitosan concentration to 3% (1.6 ± 0.24 µm).

The diameter of the PET/chitosan fiber was subsequently changed inversely (**Figure 3 and Table 1**). The little time needed to reach the collector is due to an increase in duration, which negatively impacts solvent evaporation, leading to a decrease in fiber diameter and the formation of stable electrospun fibers. The addition of chitosan may enhance the separation of extracted cellulose chains from the solvent, thus accelerating solvent evaporation. The hydrogen interaction between water molecules concurrently promotes chain entanglement, hence facilitating the spinning process. In conclusion, the amalgamation of chitosan with PET enhances the morphological characteristics and fiber diameter.

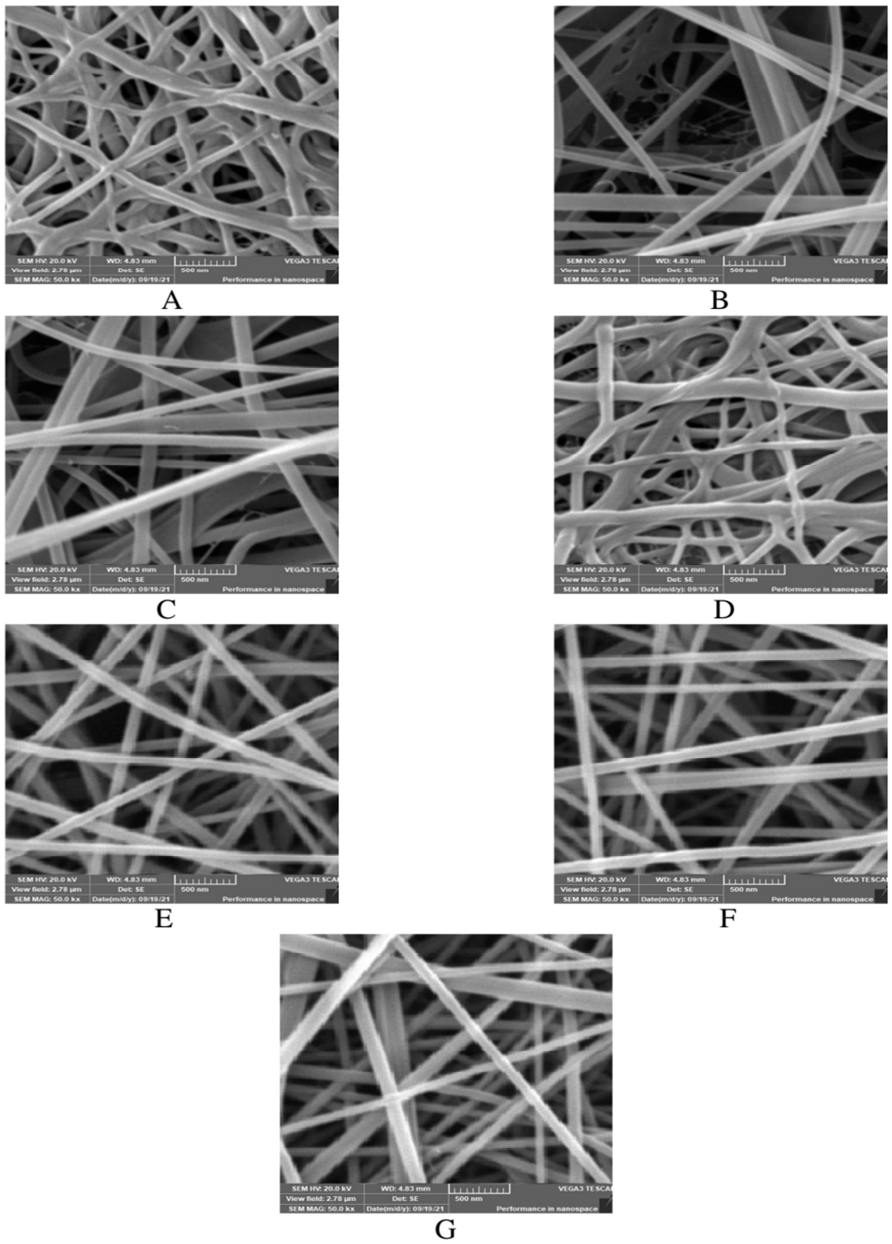

Figure 2: SEM images for produced Electro spun fibers in different solvents
A) PET(15)/TFA, B) PET(15)/TFA/DCM(50:50), C) PET (15)/TFA/DCM(70:30), D) PET(15)/DCM, E) PET (15)/Chito(1)/TFA/DCM(70:30), F) PET(15)/Chito(2)/TFA/DCM(70:30), and G) PET(10)/Chito(3)/TFA/DCM (70:30)

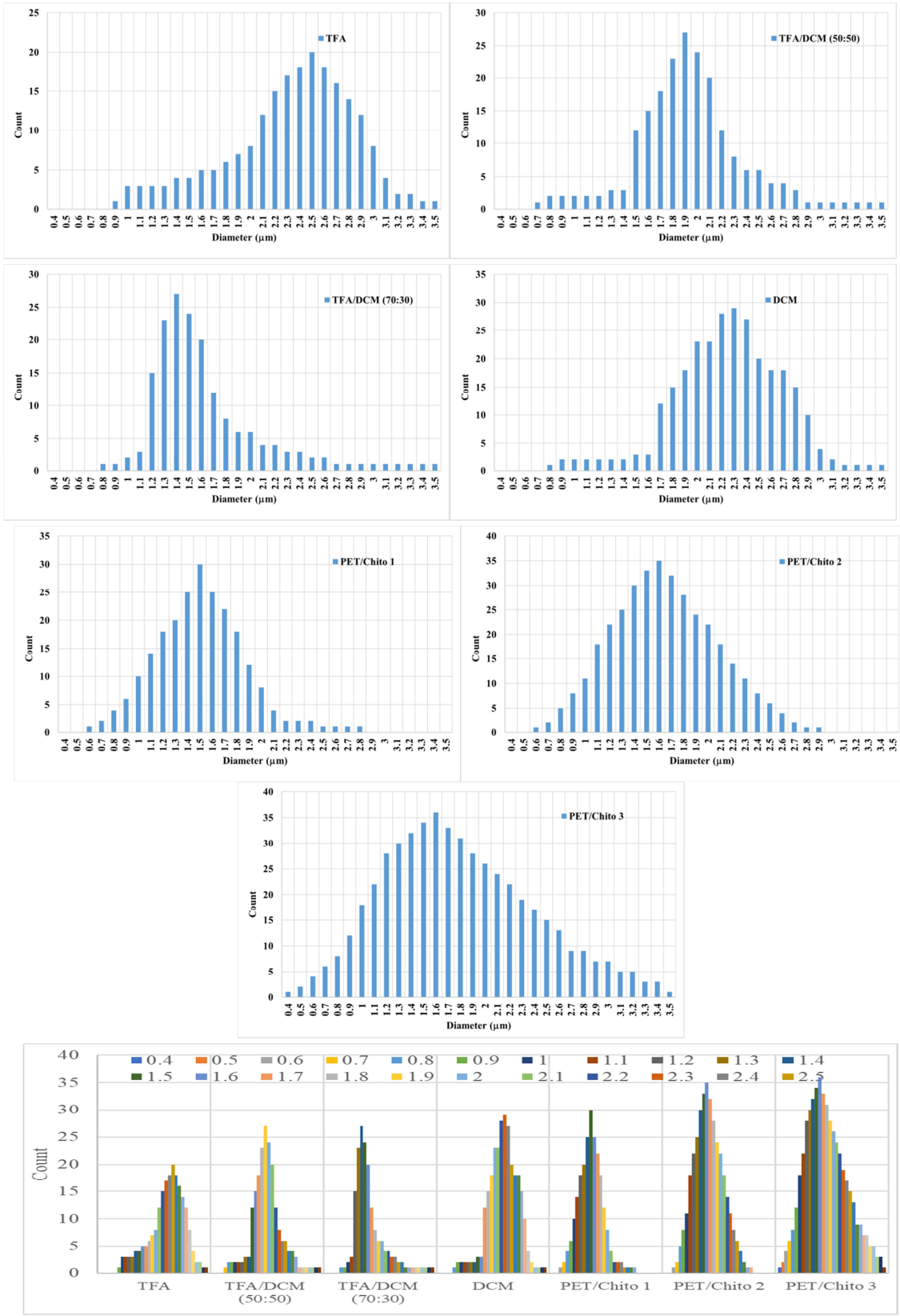

Figure 3: Diameter of produced Electro spun fibers in different solvents

Table 1: Fiber diameter of electrospun PET nanofibres

Polymer	Solvent	Conductivity (µS cm-1)	Viscosity (mPS s)	Surface tension (Nm m^{-1})	Fiber diameter (µm)	Characteristics
PET (15 %)	TFA	6.66 ± 0.74	52.33 ± 0.95	37.03 ± 4.2	2.5 ± 0.26	Thick fiber
	TFA/DCM (50:50)	7.57 ± 1.43	51.17 ± 1.08	42.17 ± 2.24	1.9 ± 0.84	Thin fiber
	TFA/DCM (70:30)	8.47 ± 1.57	50.01 ± 0.67	47.32 ± 0.45	1.4 ± 0.63	Thin fiber
	DCM	5.08 ± 0.07	48.53 ± 0.66	46.39 ± 0.06	2.3 ± 0.69	Thick fiber
PET (15 %)/ Chitosan (1%)	TFA/DCM (70:30)	5.20 ± 0.03	49.88 ± 0.11	46.37 ± 0.09	1.5 ± 0.07	Thin fiber
PET (15 %)/ Chitosan (2%)		5.24 ± 0.03	49.99± 0.12	46.25 ± 0.08	1.6 ± 0.75	Thin fiber
PET (15 %)/ Chitosan (3%)		5.27 ± 0.02	50.14 ± 0.07	46.15 ± 0.05	1.6 ± 0.24	Thin fiber

3.2. Moisture management analysis

The moisture management features of filter media significantly affect the quality and performance of the produced sample. Water exists in the atmosphere as vapor. The major objective is to create water filter media that effectively manages moisture in vapor form. This test was conducted following the AATCC 195:2017 procedure. [18]

Table 2 presents the absorption rate (%/s), wetting time (s), maximum wetted radius (mm), and spreading speed (mm/s),. All manufactured chitosan-based nanofibers exhibit excellent top-wetting times and satisfactory bottom-wetting times. Furthermore, the peak absorption rate (%/s) and the maximum wetted radius (mm) are of substandard quality. Although the nanofibrous membrane is derived from recycled polyethylene terephthalate, resulting in suboptimal moisture management capabilities, the use of chitosan inside the PET matrix enhances these characteristics.

Table 2: Moisture management properties of produced electrospun nanofibers based on PET/Chitosan

Parameters	PET/Chitosan 1 surface		PET/Chitosan 2 surface		PET/Chitosan 3 surface	
	Top	Bottom	Top	Bottom	Top	Bottom
Wetting time (s)	7.747± 0.11	7.939± 0.01	6.568± 0.11	6.359± 0.13	5.258± 0.07	5.592± 0.12
Absorption rate (%/s)	4.669± 0.12	4.332± 0.11	5.336± 0.21	5.809± 0.01	5.896± 0.12	5.208± 0.11
Maximum wetted radius (mm)	4.576± 0.01	4.576± 0.21	5.230± 0.82	5.230± 0.02	5.779± 0.11	5.779± 0.32
Spreading speed (mm/s)	0.648± 0.01	0.74± 0.02	0.740± 0.03	0.84± 0.05	0.818± 0.07	0.93± 0.04

3.3. Adsorption Study

The PET/Chitosan nanofibre may interact with each metal salt via hydrogen bonding and/or hydrophilic-hydrophobic interactions. This observation may be ascribed to the reduction in metal salt dissociation, resulting in a diminished concentration of dye species accessible to engage with the nanofibre active sites. This behavior can be elucidated by the reduced degree of protonation of functional groups, specifically amino groups.

The heavy metals uptake was determined by the difference in metal salt concentrations in the supernatant, utilizing the equation:

$$Q = V(C_o - C_f) / M$$

In this equation, Q represents the metal salt uptake (mg/g), C_o and C_f denote the beginning and final metal salt concentrations in the solution (mg/l), respectively, V signifies the volume of the solution (L), and M indicates the weight of the nanofibre (g).

3.3.1. Effects of the contact time on the adsorption of metal salts onto nanofibersurface

Figure 5 shows the dye Concentration as a function of time at an initial dye concentration of 40 mg, efficiency of dye adsorption (%), and Adsorbed Dye Concentration (mg dye/mg fiber) in the uptake of RB5 and MB respectively by the nanofibre. It was observed that about 95% of the total uptake of RB5 could be achieved within 60 min.

The graph in Figure 4 shows the dye concentration vs time at an initial concentration of 40 mg, the efficiency of dye adsorption in percentages, and the adsorbed dye concentration in milligrams per milligram of fiber for the nanofiber's uptake of RB5 and MB, respectively. Within 60 minutes, approximately 95% of the total uptake of RB5 could be accomplished.

At an initial concentration of 40 mg, the graph in **Figure 4** and

Figure 5 illustrates the relationship between various metal salt concentrations ($Ba(NO_3)_2$, $Mn(NO_3)_2$, $Co(NO_3)_2$ and $Ni(NO_3)_2$) and time. Additionally, the graph displays the efficiency of metal salts adsorption expressed as a percentage, as well as the adsorbed metal salts concentration expressed in milligrams per one gram of nanofiber for the nanofiber's uptake. Within sixty minutes, it is possible to achieve approximately ninety-five percent of the total uptake of heavy metal salts.

Figure 4 shows how the concentration of different metal salts changes over time when they are adsorbed (stuck) onto the surface of different nanofibers. This graph likely illustrates how quickly or slowly various metals attach to the nanofibers and how the concentration of these metals in solution decreases as they are removed by the nanofibers.

Figure 5 displays the efficiency of metal ion adsorption for different metal salts onto various nanofiber surfaces. This graph probably compares how well different nanofibers can remove specific metal ions from a solution, expressed as a percentage. A higher percentage would indicate that the nanofiber is more effective at removing that particular metal from the solution.

These figures are likely part of a study investigating the use of nanofibers for removing metal contaminants from water or other solutions, which could have applications in environmental cleanup or water purification technologies.

3.4. Kinetic Study

The kinetics of adsorption processes provide valuable insights into adsorption efficiency and the viability of scaling operations. The concentration-time curves (**Figure 4**) for the adsorption of different heavy metal salts onto different nanofiber surfaces indicate that each heavy metal salts are effectively adsorbed by all produced nanofibers, depleting approximately 90 % of the heavy metal salts bath effluent. [5, 10, 30-34]

Three kinetic models were evaluated to determine the suitable expression for the adsorption rate: the pseudo-first-order model [35], the pseudo-second-order model [36], and the Intra-particle diffusion model [37]. The equation for the pseudo-first-order rate is presented below:

$$\frac{dq}{dt} = k_1(q_e - q_t)^n$$

Let the amount of dye adsorbed (mg/g) at time t be denoted as the maximal adsorption capacity (mg/g), k as the rate constant (min), and n as the reaction order. The linear form can be expressed in terms of integration as follows:

$$\ln(q_e - q_t) = \ln(q_e) - k_1 t \quad \text{For n=1 (first-order response)}$$

The rate of the pseudo-second-order model is contingent upon the quantity of dye adsorbed on the adsorbent's surface and the amount adsorbed at equilibrium [26]. After integration, the model was articulated as:

$$\frac{1}{q_t} = \left(\frac{1}{k_2 q_e^{\,2}}\right)\left(\frac{1}{t}\right) + \frac{1}{q_e}$$

In this context, qt represents the quantity of dye adsorbed (mg/g) at time t, qe denotes the maximal adsorption capacity (mg/g) for second-order adsorption, and k2 signifies the second-order rate constant (g/mg.min).

Neither the pseudo-first-order nor the pseudo-second-order models can only identify the diffusion mechanism; thus, the intra-particle diffusion model was introduced. The initial rate of the intra-particle equation is as follows [37]:

$$Q_t = K_d t^{(1/2)} + C$$

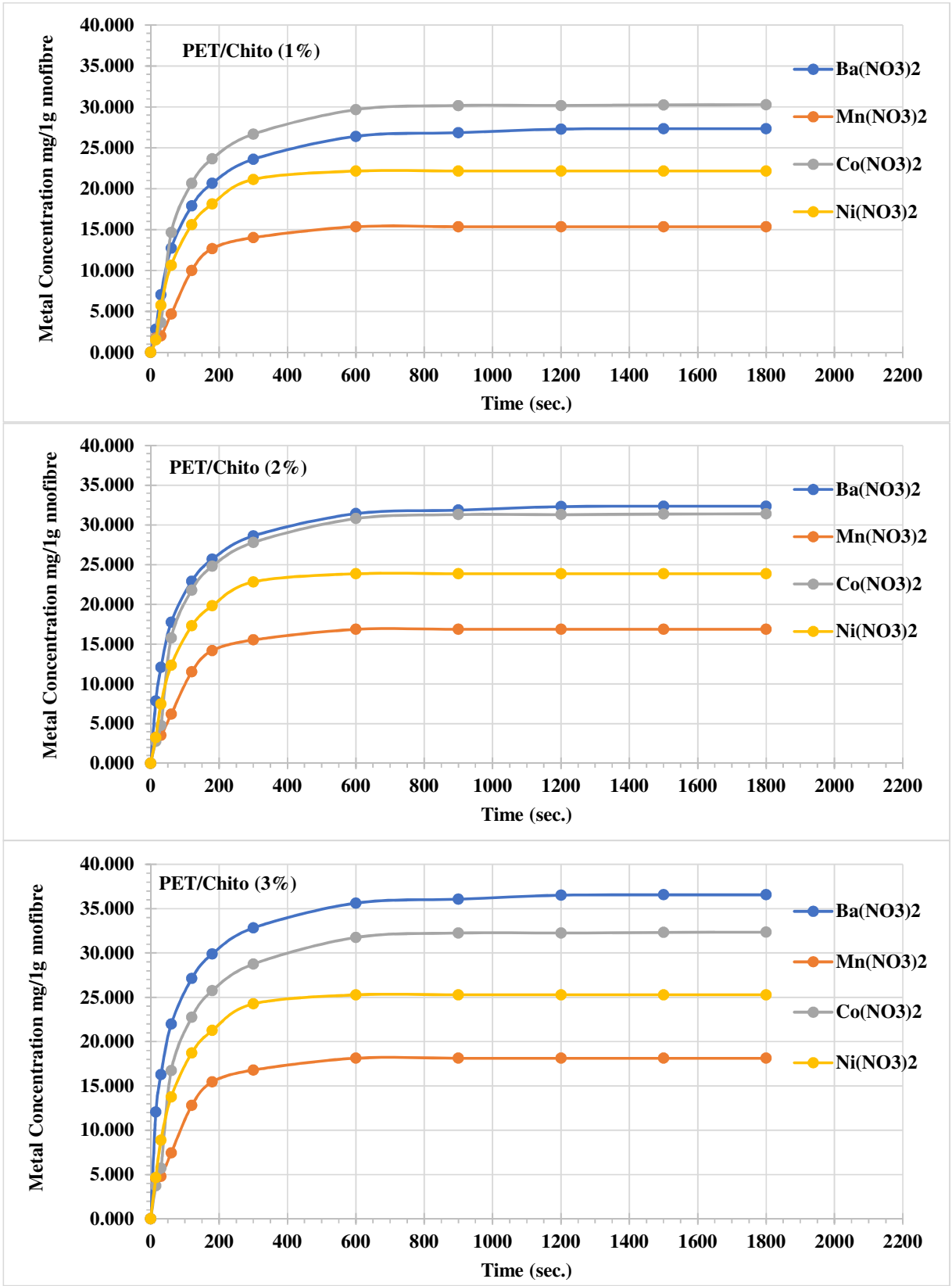

Figure 4: The concentration-time curve of different metal salts onto the surface of different nanofibre

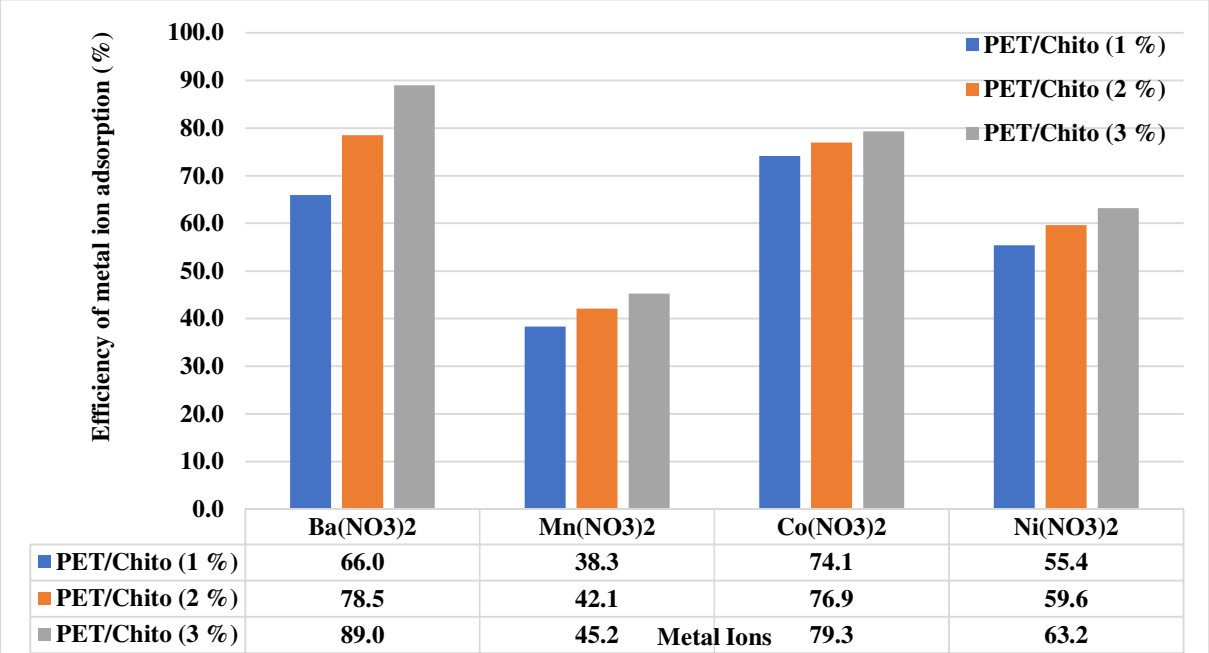

Figure 5: Efficiency of metal ion adsorption (%) of different metal salts onto the surface of different nanofibre

In this context, K_d represents the intra-particle rate constant (g/mg $min^{-1/2}$), which is dependent on the equilibrium concentration in the solid phase, Q_t, and the intra-particle diffusion C may be ascertained. The adsorption rate constant (K) values for heavy metal salts adsorption on each PET/Chitosan nanofiber nanofibre were calculated from the aforementioned formulae. Furthermore, the values of additional parameters and the correlation coefficient were computed for each plot. The reaction order was selected based on the optimal linear correlation, shown by the highest R^2 value. The values of the rate constant (K) and correlation coefficients are presented in **Table 3**.

Table 3 demonstrates that the pseudo-second-order kinetics model provides the optimal match for the adsorption data of all heavy metal salts by each produced PET/Chitosan nanofiber. The pseudo-second-order kinetic model indicates that the adsorption mechanism is diffusional, occurring through micropores. Furthermore, the results presented in **Table 3** demonstrate that the pseudo-first-order kinetics model provides the optimal fit for the adsorption data of heavy metal salts by each synthesized PET/Chitosan nanofiber. The pseudo-first-order kinetic model indicates that the adsorption mechanism is diffusional, occurring through micropores (**Figure 6**, **Figure 7**, **Figure 8**, and **Figure 9**).

Nonetheless, the plots of each heavy metal uptake Qt against the square root of time $t^{1/2}$ do not intersect the origin in our investigation. This suggests that intraparticle diffusion is not the only rate-limiting phase in the sorption process; other kinetic processes may also be occurring and contributing to the sorption mechanism. [37]

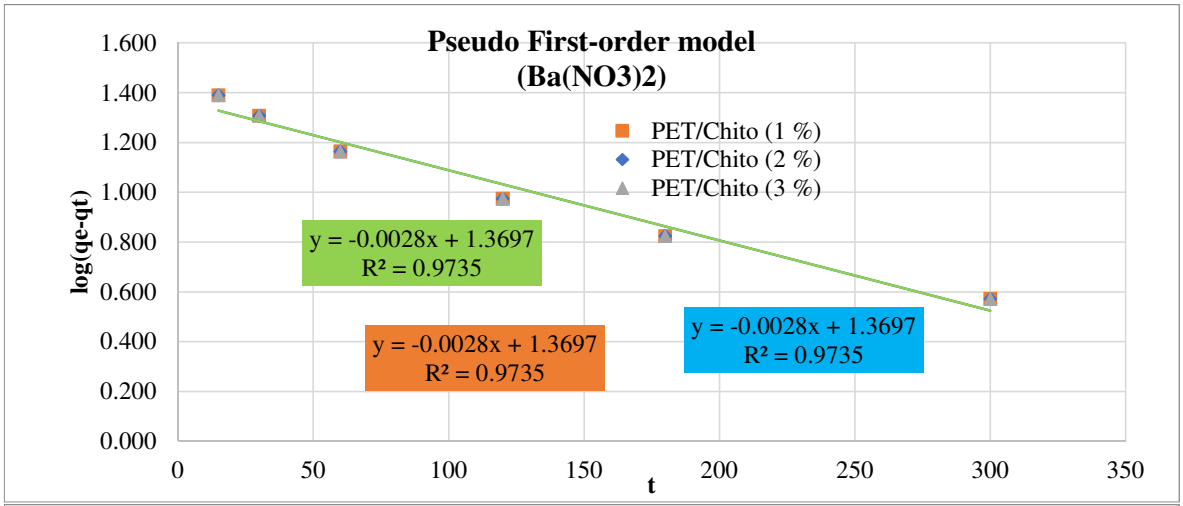

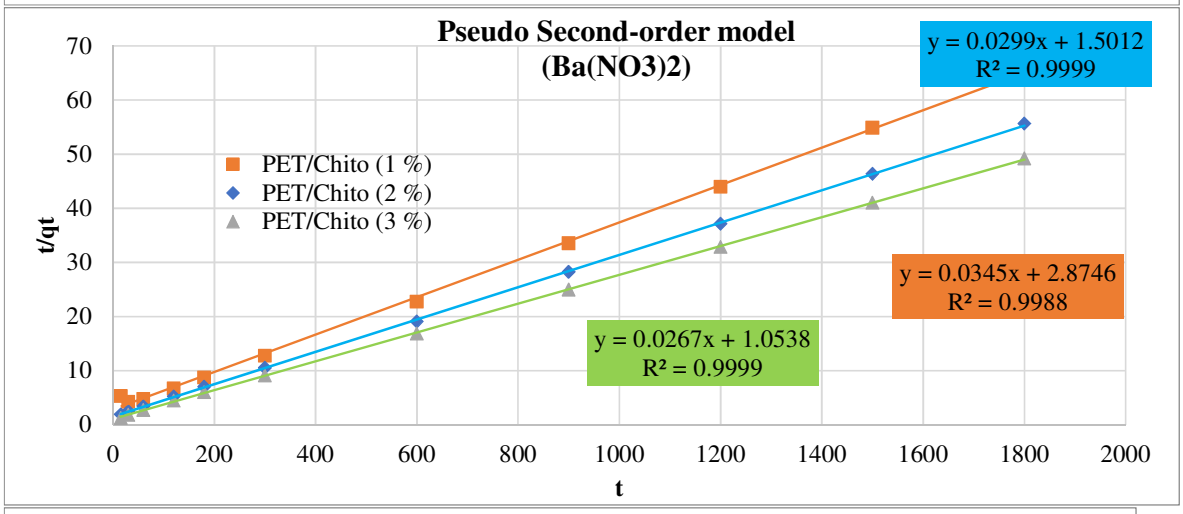

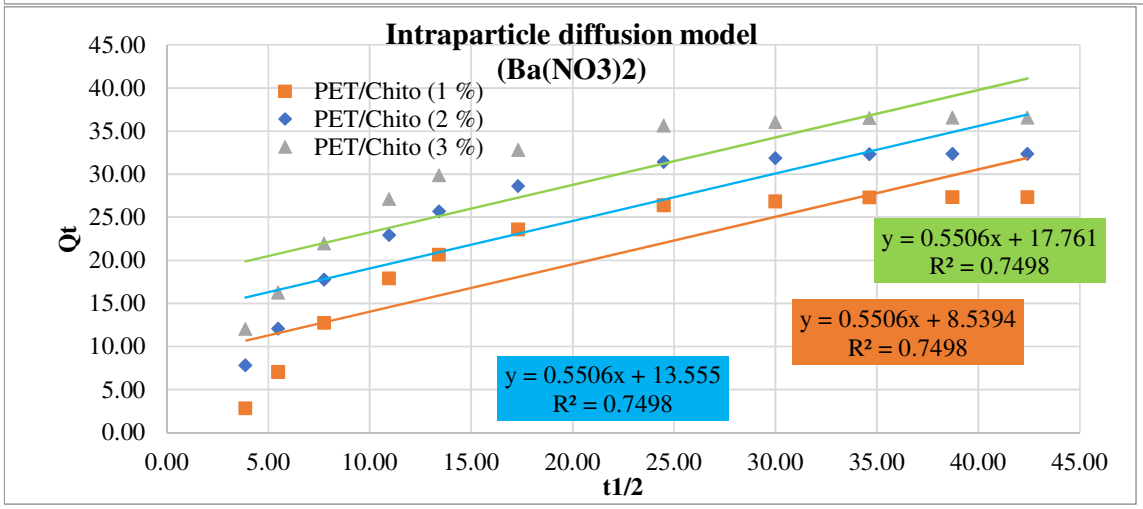

Figure 6: Adsorption models of kinetic parameter for $Ba(NO_3)_2$ onto the surface of different nanofibre

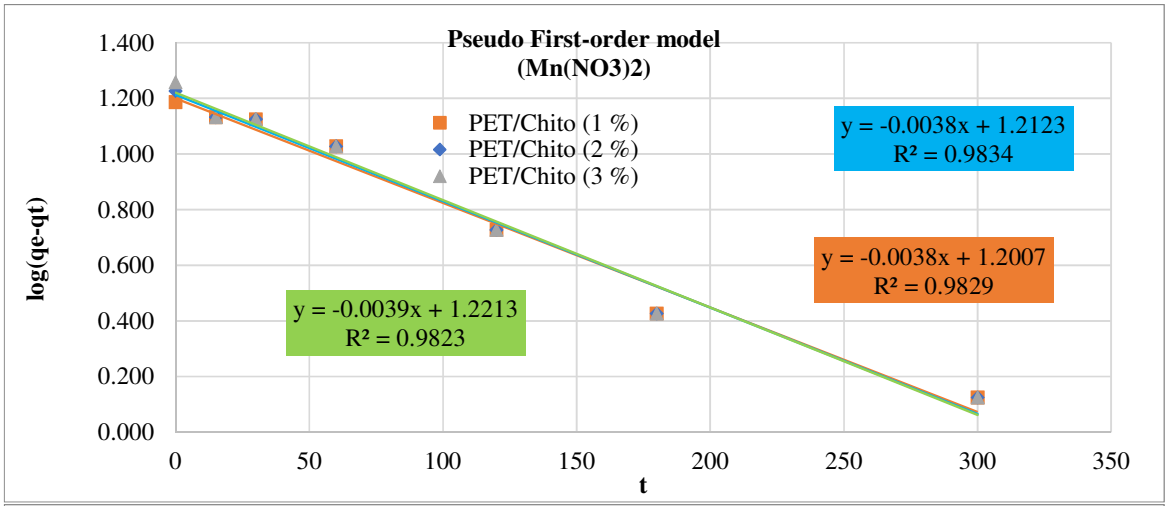

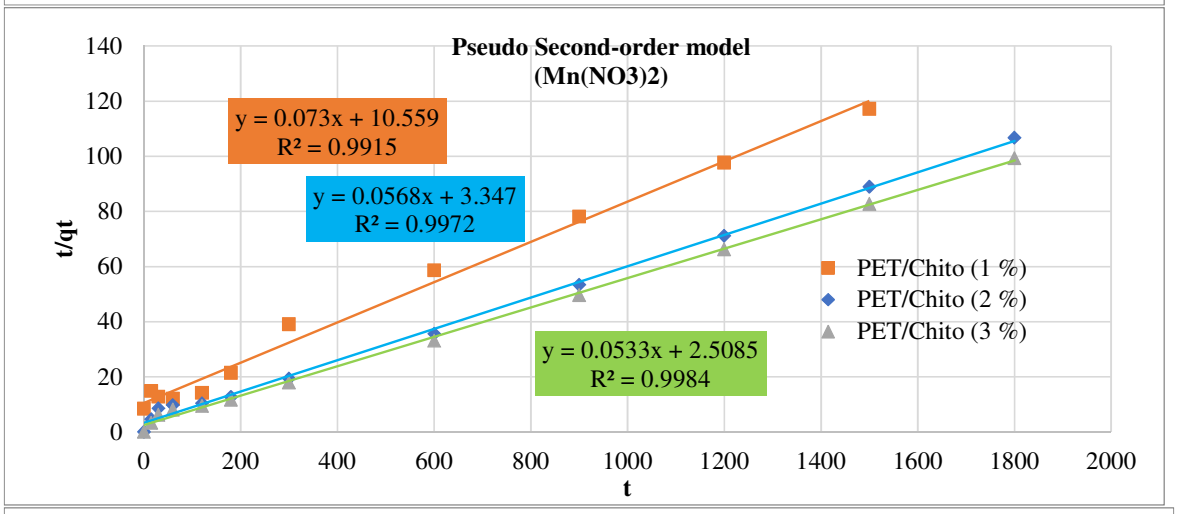

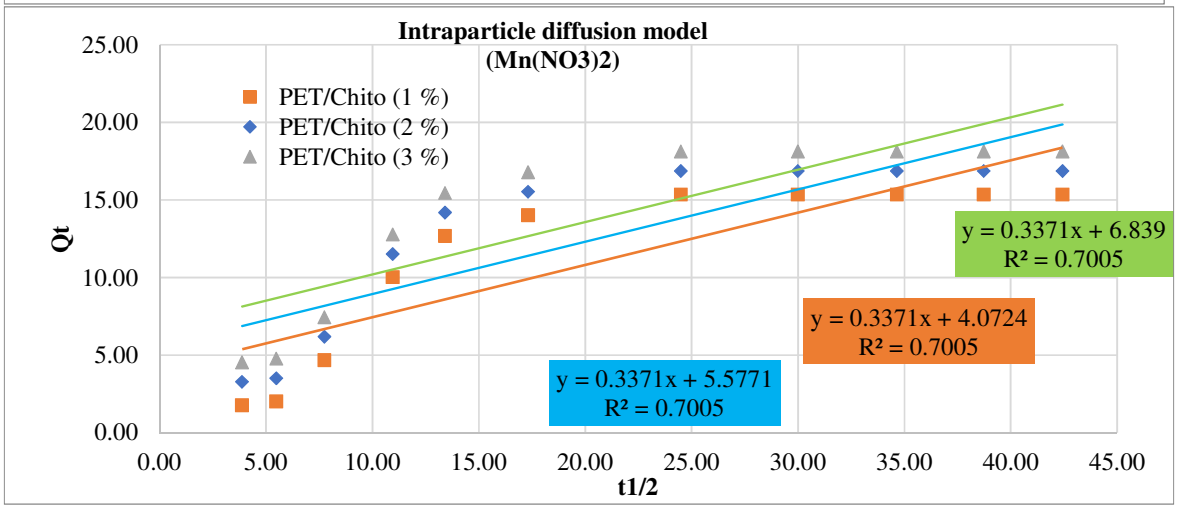

Figure 7: Adsorption models of kinetic parameter for $Mn(NO_3)_2$ onto the surface of different nanofibre

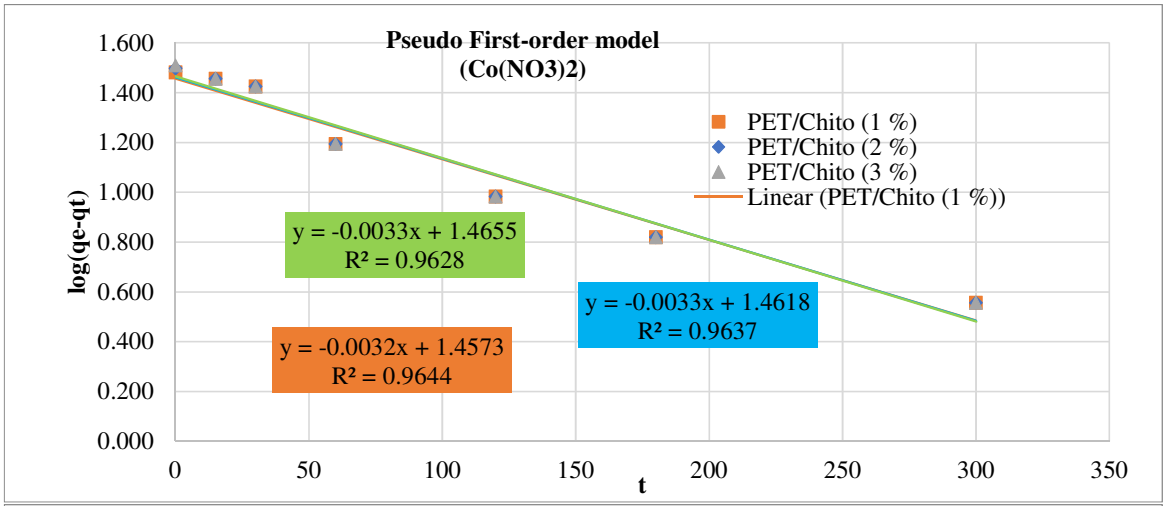

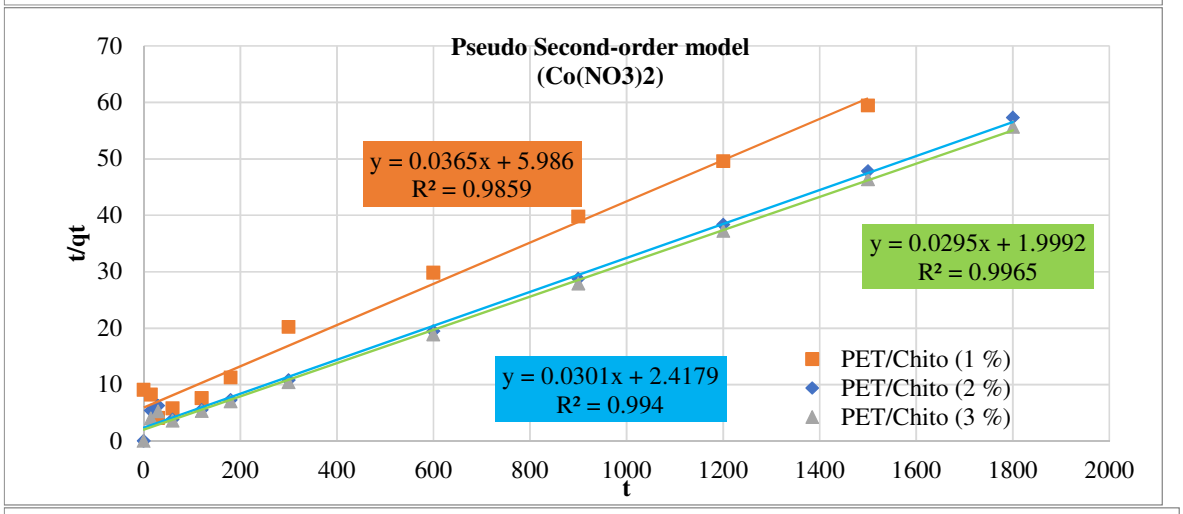

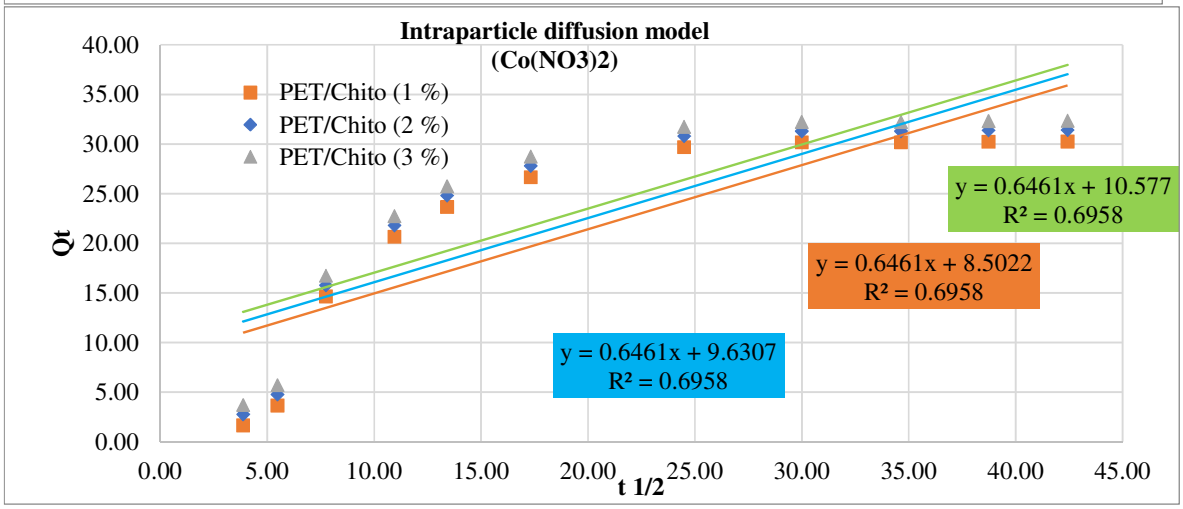

Figure 8: Adsorption models of kinetic parameter for $Co(NO_3)_2$ onto the surface of different nanofibre

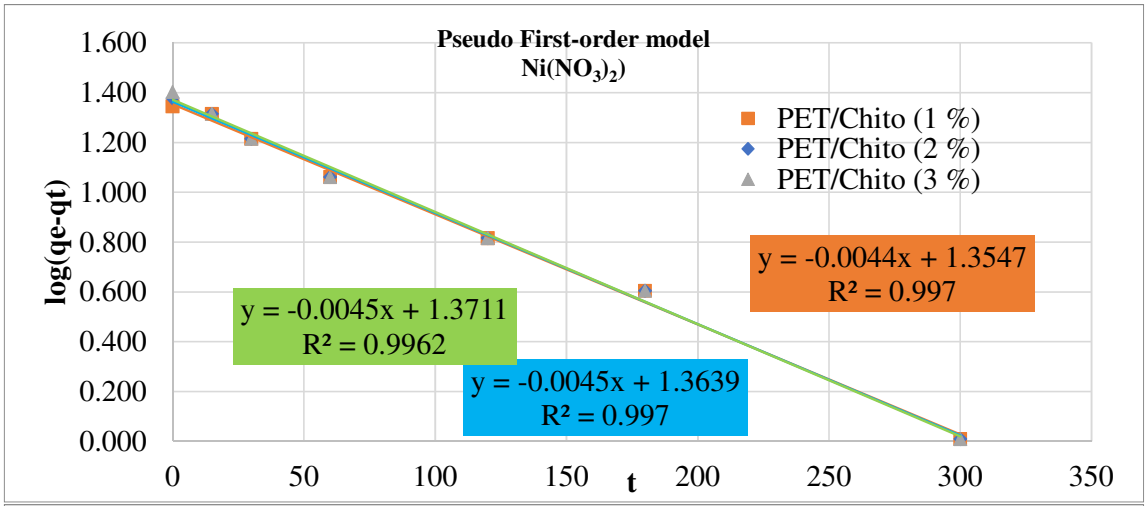

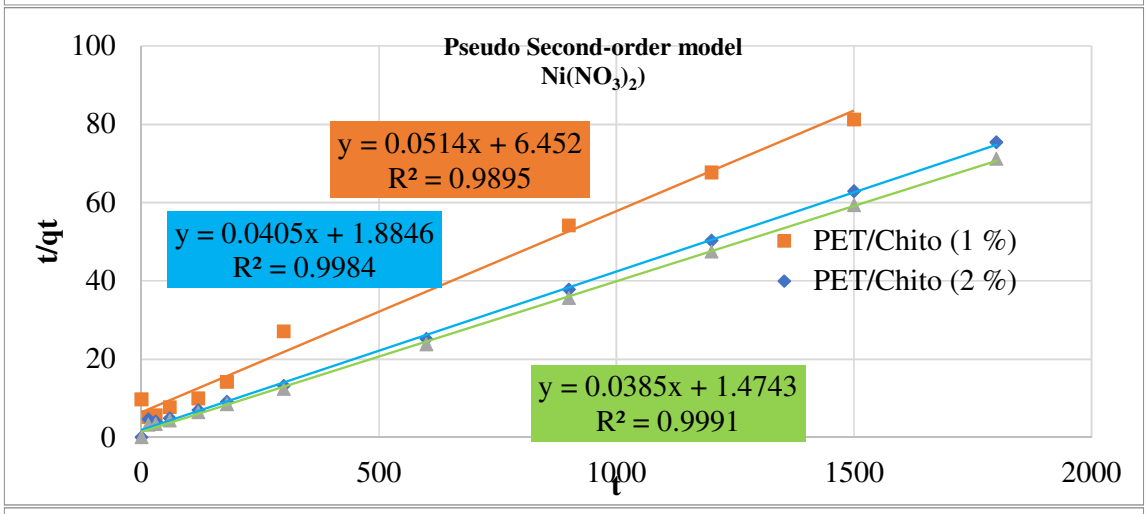

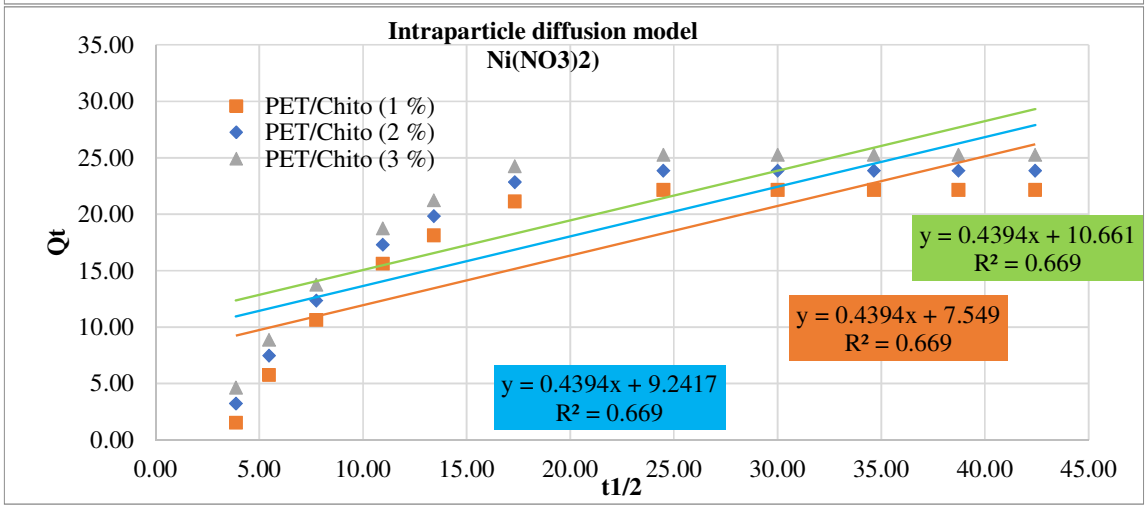

Figure 9: Adsorption models of kinetic parameter for $Nl(NO_3)_2$ onto the surface of different nanofibre

Table 3: The kinetic parameters values as obtained from the experimental data for various heavy metal salts using different nanofibers

Nanofiber	Parameters	Kinetic Models											
		Ba $^{+2}$			Mn $^{+2}$			Co $^{+2}$			Ni $^{+2}$		
		Pseudo First-order	Pseudo Second-order	Intraparticle diffusion	Pseudo First-order	Pseudo Second-order	Intraparticle diffusion	Pseudo First-order	Pseudo Second-order	Intraparticle diffusion	Pseudo First-order	Pseudo Second-order	Intraparticle diffusion
PET/Chito 1 %	R^2	0.9781	**0.9988**	0.7498	0.9802	**0.9935**	0.7005	0.9575	**0.9863**	0.6958	0.9945	**0.9960**	0.6689
	K	0.0048	0.0004	0.5506	0.0087	0.0006	0.3371	0.0073	0.0002	0.6461	0.0102	0.0005	0.4393
	C			8.5406			4.0725			8.5025			7.5485
	Q_e	19.8765	28.9487		16.0833	16.6234		28.0329	33.2740		22.8220	23.5875	
PET/Chito 2 %	R2	0.9781	**0.9999**	0.7498	0.9802	**0.9979**	0.7005	0.9575	**0.9952**	0.6958	0.9965	**0.9988**	0.6689
	K	0.0048	0.0006	0.5506	0.0087	0.0008	0.3371	0.0074	0.0003	0.6461	0.0102	0.0007	0.4394
	C			13.557			5.5772			9.6310			9.2411
	Qe	19.8765	33.4557		16.0833	17.7629		28.0329	33.6400		22.8220	24.8622	
PET/Chito **3 %**	R2	0.9781	**0.9999**	0.7498	0.9802	**0.9989**	0.7005	0.9575	**0.9974**	0.6958	0.9965	**0.9994**	0.6689
	K	0.0048	0.0007	0.5506	0.0087	0.0009	0.3371	0.0074	0.0004	0.6461	0.0102	0.0008	0.4393
	C			17.7639			6.8392			10.5775			10.6607
	Qe	19.8765	37.5244		16.0833	18.8917		28.0329	34.2706		22.8220	26.1474	

3.1. Isothermal Studies

UV-vis spectrophotometry is used to determine the maximum sorption capacities at various initial heavy metal salt concentrations. The results are displayed in (**Figure 11** and **Figure 10**) as adsorbed heavy metal salts concentration (mg/g) or heavy metal salts adsorption efficiency (%) plotted against different initial heavy metal salts concentrations. These figures demonstrate that as the heavy metal salts concentration in the effluent bath increases from 1 to 1000 mg/L, the maximum adsorbed heavy metal salts concentration rises correspondingly with higher chitosan content in the nanofibres (1 - 3%). However, when calculating the heavy metal salt adsorption efficiency (%), a notable inverse relationship is observed.

Specifically, the heavy metal salts adsorption efficiency decreases as the heavy metal salts amount increases, showing varying values up to 400 mg/L. Beyond this point, further increases in heavy metal salt concentration lead to a continued decline in adsorption efficiency.

Figure 10 shows the amount of heavy metal salts absorbed per gram of material (adsorption capacity). **Figure 11** shows the percentage of heavy metal salts that are absorbed (adsorption efficiency).

The study looks at how well PET with different amounts of chitosan (1-3%) in nanofibres can absorb heavy metal salts. As more heavy metal salts are added to the solution (from 1 to 1000 mg/L), materials with more chitosan can absorb a larger amount of these salts. However, the percentage of salts absorbed (efficiency) decreases as more salts are added to the solution. The adsorption efficiency varies up to 400 mg/L of salt concentration. After this point, adding more salts continues to decrease the absorption efficiency. In simple terms, while PET with more chitosan can absorb more heavy metal salts overall, it becomes less efficient at removing all of the salts from the solution as the concentration increases.

The adsorption isotherm can also be illustrated using the curve of adsorbed various heavy metal salt concentrations, which helps explain how nanofibers interact with various heavy metal salts. [32, 38] Various models describe adsorption isotherms, with Langmuir, Freundlich, BET, and Dubinin-Radushkevich being the most commonly applied to textile fibers. [32, 38]

For single-solute systems, the Langmuir isotherm is frequently used. [39] This model assumes that intermolecular forces rapidly decrease as distance increases, resulting in a prediction of monolayer heavy metal salt coverage on the nanofibers' exterior surface. Additionally, it presumes that adsorption takes place at specific, uniform sites on the nanofiber surface, with minimal interaction between adsorbed species. The Langmuir isotherm is represented by the following equation:

$$q_e = \frac{q_m C_e K_L}{1 + C_e K_L}$$

In this context, qe represents the equilibrium heavy metal salts concentration on the nanofiber (mg/g), C_e denotes the equilibrium heavy metal salts concentration in the solution (mg/L), q_m stands for the maximum capacity of the PET/Chitosan nanofibers (mg/g), and K_L is the Langmuir adsorption constant (L/mg). By reorganizing the components of the aforementioned equation, a linear form of the Langmuir isotherm can be expressed as shown in the subsequent equation. Graphing $1/q_e$ against $1/C_e$ yields a linear relationship, with $1/q_eK_L$ as the slope and $1/q_m$ as the y-intercept.

$$\frac{1}{q_e} = \frac{1}{q_m} + \left(\frac{1}{q_m K_L}\right)\left(\frac{1}{C_e}\right)$$

The Freundlich isotherm is well-suited for characterizing heterogeneous systems. [39] This empirical model was used to examine the adsorption of various heavy metal salts onto PET/Chitosan nanofibres surfaces. The Freundlich isotherm is expressed by the following equation:

$$q_e = K_F C_e^{1/n}$$

In this equation, q_e represents the equilibrium of heavy metal salts concentrations on the PET/Chitosan nanofibres-surface (mg/g), C_e denotes the equilibrium heavy metal salts concentrations in solution (mg/L), K_F is the Freundlich adsorption constant (L/mg), and n signifies the heterogeneity factor. The linearized form of the Freundlich isotherm is presented in the equation below. Plotting Ln(qe) against Ln(C_e) yields a straight line with a slope of 1/n and an intercept of Ln(K_F).

$$\ln q_e = \ln K_F + \frac{1}{n} \ln C_e$$

The Brunauer-Ernmett-Teller (BET) isotherm model was the third model used in this research. [40] It was applied to interpret the adsorption data, and its linear form is expressed as:

$$C_f = \frac{(K_b - 1)(K_b C_{\max} C_s) + K_b C_{\max} C_i}{(C_i - C_s)(K_b - 1)}$$

Where C_f denotes the dye concentration adsorbed on the PET/Chitosan nanofibres surface, Cs represents the heavy metal salts concentration in the effluent bath, C_{max} indicates the maximum adsorption capacity of the heavy metal salts onto the PET/Chitosan nanofibres (mg/g), C_i signifies the saturation concentration of heavy metal salts (mg/L), and K_b is the constant that characterizes the energy of interaction with the PET/Chitosan nanofibres surface. The linear equation for the Brunauer-Emmett-Teller (BET) isotherm is:

$$\frac{C_s}{(C_i - C_s)C_f} = \frac{1}{K_b C_{\max}} + \left(\frac{K_b - 1}{K_b C_{\max}} \right) \left(\frac{C_s}{C_i} \right)$$

The graph of ($C_s/(C_i - C_s)C_f$) against (C_s/C_i) yields a linear relationship characterized by a slope of ($(K_b - 1)/(K_b \times C_{\max})$) and an intercept of ($1/(K_b - 1)$).

Additionally, the experimental results were analyzed using the Dubinin–Radushkevich (D–R) model to ascertain if the adsorption process was physical or chemical in nature. The D–R equation is more comprehensive than the Langmuir model since it does not presuppose a homogenous surface, a constant sorption potential, or the lack of a steric barrier between adsorbed and incoming particles. The linear representation of this model is expressed by the following equation.

$$\ln q_e = \ln q_m - \beta \varepsilon^2$$

In this context, q_e (mmol/g) denotes the quantity of heavy metal salts adsorbent per gram of PET/Chitosan nanofibers, while q_m (mmol/g) signifies the maximum sorption capacity of the adsorbent. The constant β ($mol^2.kJ^{-2}$) pertains to the energy of sorption, and ε represents the Polanyi sorption potential, which is computed using the subsequent equation:

$$\varepsilon = RT \ln (1 + \frac{1}{C_e})$$

Here, R denotes the gas constant, valued at 8.314 $J \cdot mol^{-1} \cdot K^{-1}$, T represents the temperature in Kelvin, and C_e (M) signifies the equilibrium concentration of the heavy metal salt. The Polanyi sorption model posits a constant volume of sorption space next to the sorbent surface and the presence of a sorption potential within these regions. The sorption space surrounding a solid surface is defined by a succession of equipotential surfaces that possess identical sorption potential. The sorption potential is temperature-independent but changes based on the characteristics of the sorbent and sorbate.

The parameters β and q_m were derived from the slope and intercept of the Lnq_e against the ε^2 plot. The mean free energy of sorption E (kJ mol^{-1}) necessary to transport one mole of heavy metal salt from infinity in the solution to the surface of PET/Chitosan nanofibers may be calculated using the following equation:

$$E = (-2\beta)^{-\frac{1}{2}}$$

Every parameter value obtained from curve fits using the aforementioned four adsorption isotherms are enumerated in **Table 4**. The Dubinin–Radushkevich isotherm is typically utilized to characterize the adsorption mechanism with a Gaussian energy distribution on a heterogeneous surface. The method was often employed to differentiate between the physical and chemical adsorption of four heavy metal salts ($Ba(NO_3)_2$, $Mn(NO_3)_2$, $Co(NO_3)_2$, and $Ni(NO_3)_2$) in their aqueous solutions, utilizing the mean free energy, E, per molecule of adsorbate (for relocating a molecule from its position in the sorption space to infinity). The mean free energy, E values, rose with the concentration of chitosan in the nanofibers for heavy metal salts utilized. The E values were 0.06, 0.090.03, and 0.06 kJ/mol for $Ba(NO_3)_2$, $Mn(NO_3)_2$, $Co(NO_3)_2$, and $Ni(NO_3)_2$, respectively, even increasing in the chitosan content in the nanofiber from 1 to 3%, denoting a chemo-sorption process. [41]

The Freundlich adsorption model demonstrates superior alignment with the experimental data, as seen by its higher R^2 correlation coefficients compared to other models. Furthermore, the adherence to the Freundlich model indicates that all

heavy metal salts may adsorb onto the active regions of the PET/Chitosan nanofibers, resulting in multilayer coverage. Moreover, since the n value from the Freundlich model exceeds 1, it indicates favorable adsorption conditions. [42]

A value of n greater than 1 indicates favorable adsorption across all concentrations, with uptake increasing as the concentration increases. When n is less than 1, adsorption is a chemical process; when n is equal to 1, adsorption is linear; and when n is greater than 1, adsorption is a physical process. [43]

As shown in **Table 4**, all n values are <1, indicating a favorable chemical adsorption process for the removal of heavy metal salts. As seen in **Table 4**, the Freundlich isotherm model also fits the experimental better than the Langmuir's model (correlation coefficient R2 > 0.99), whereas, the Langmuir has low correlation coefficients. As the PET/Chitosan nanofibers adsorbent used in the present studies is a non-conventional adsorbent, its capacity has been compared with other non-conventional adsorbents. [5, 6, 10, 13, 44, 45]

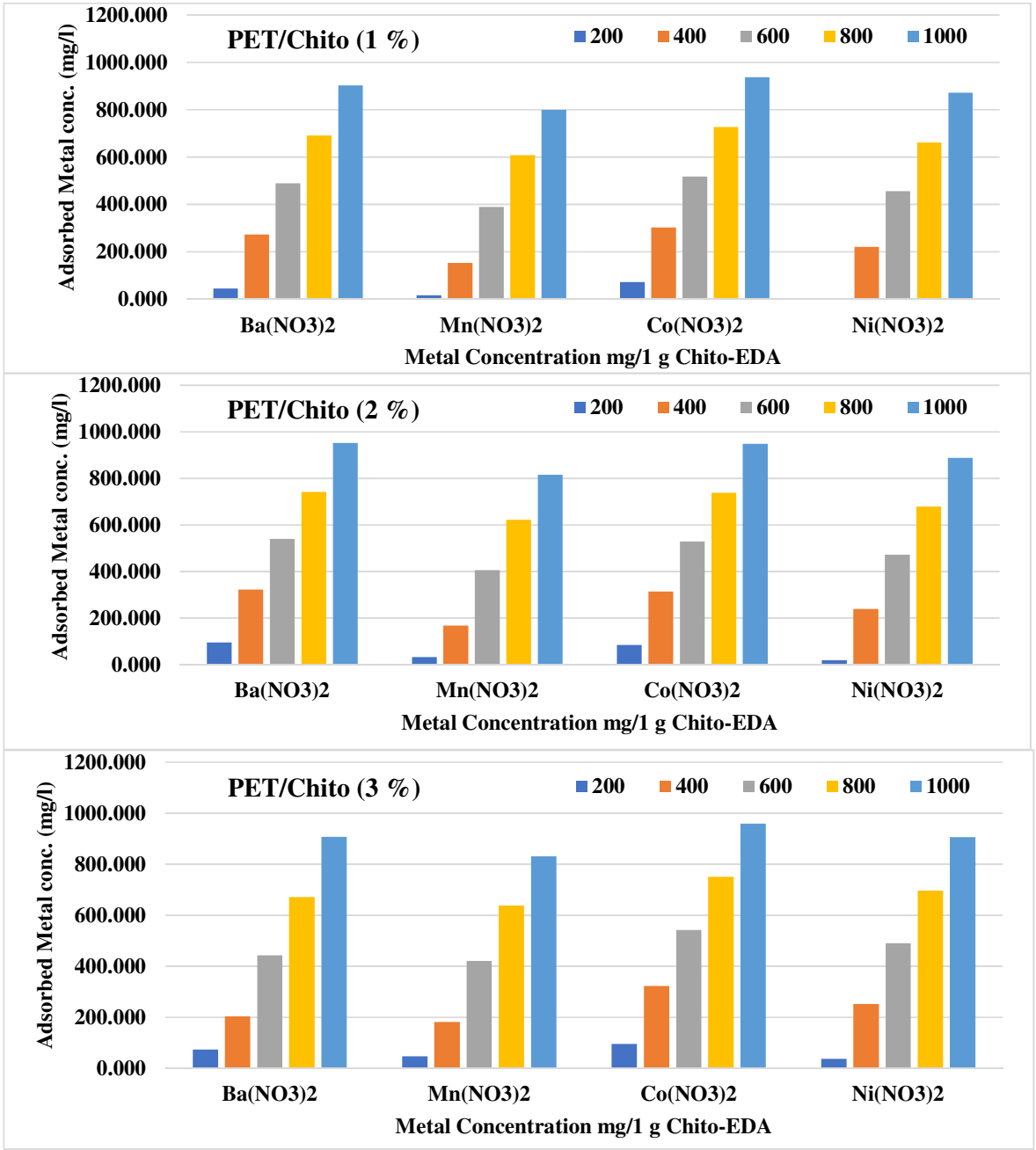

Figure 10: Adsorbed metal salts Concentration onto the surface of different PET/Chitosan nanofibre

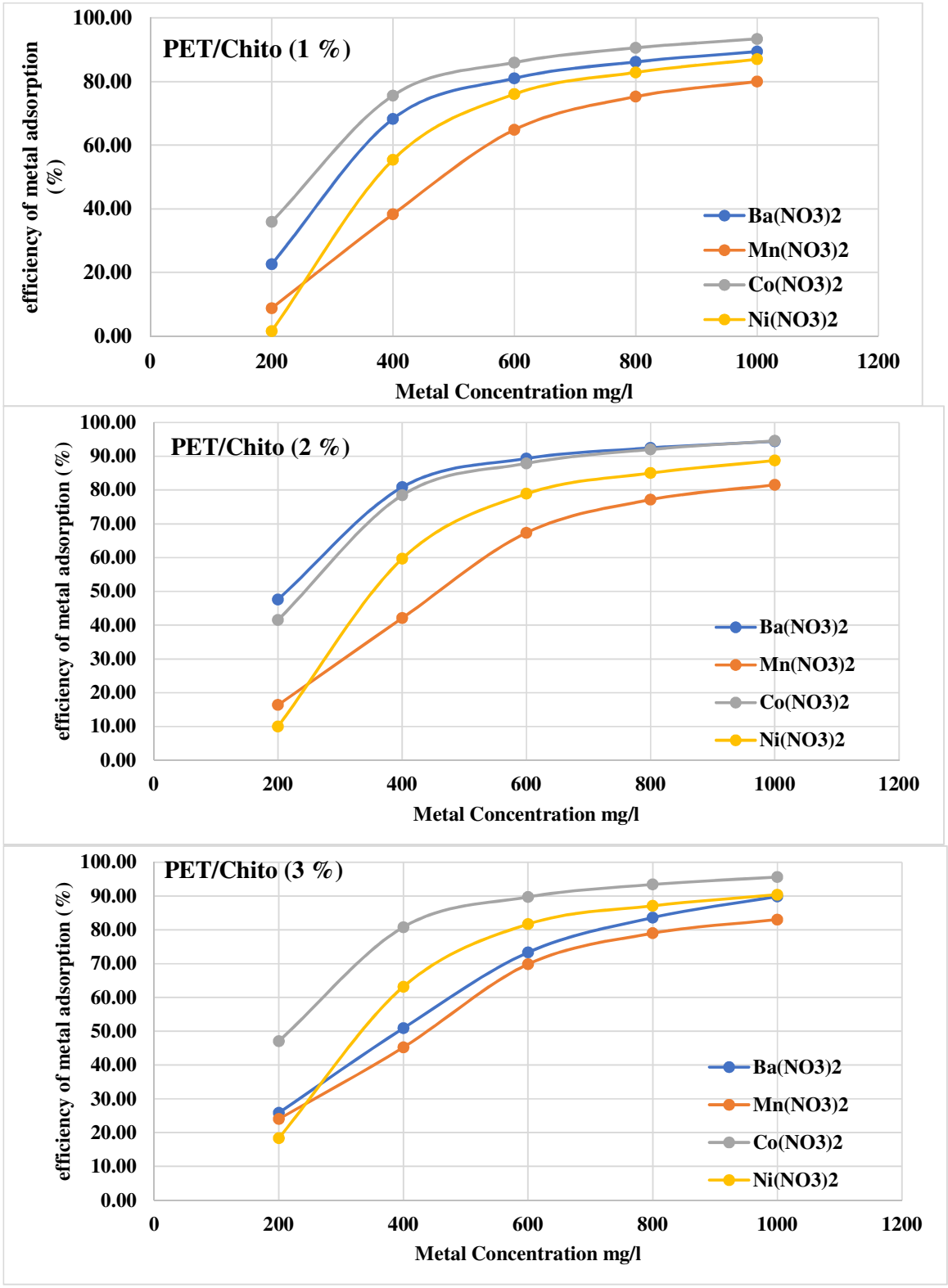

Figure 11: efficiency of metal salts adsorption (%)onto the surface of different PET/Chitosan nanofibre

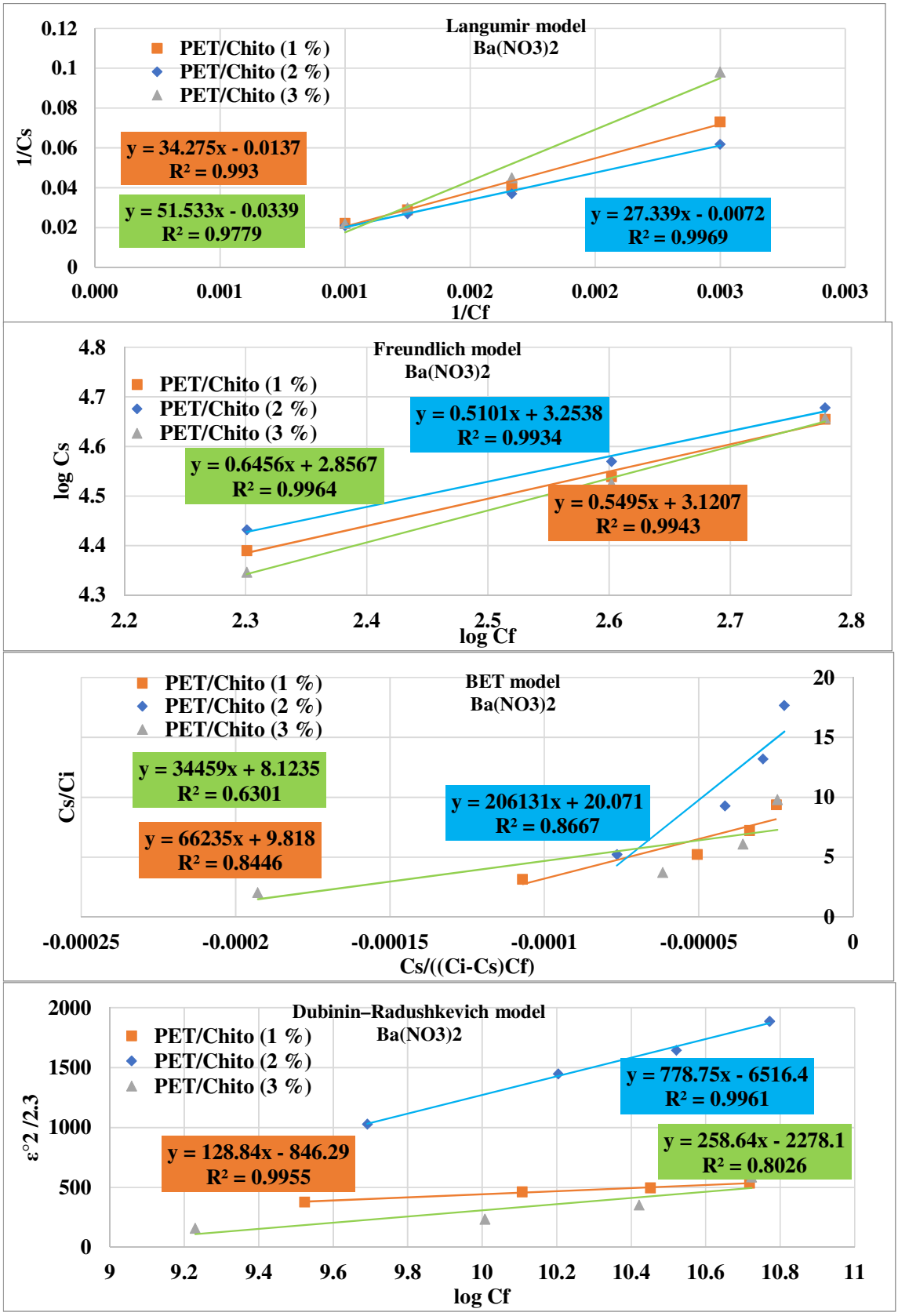

Figure 12: Isothermal models for **$Ba(NO_3)_2$**using different used nanofibres

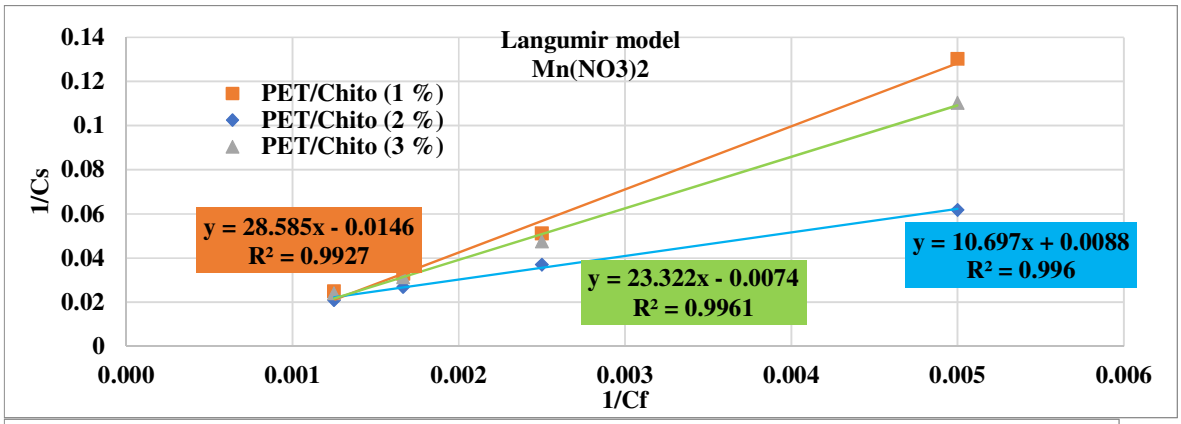

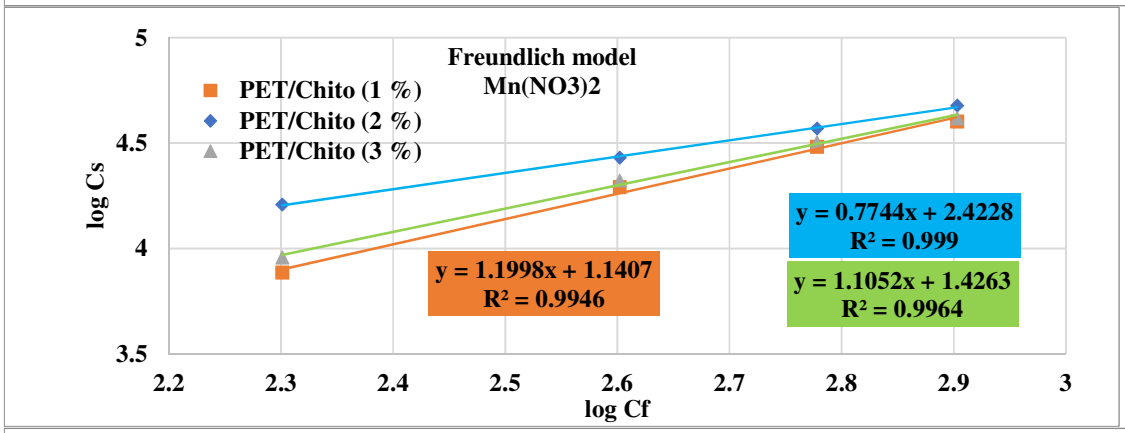

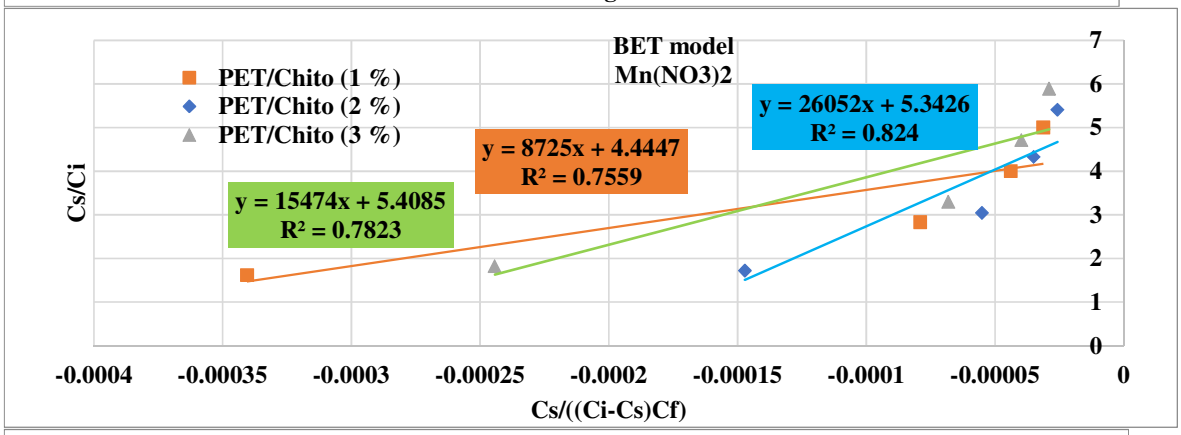

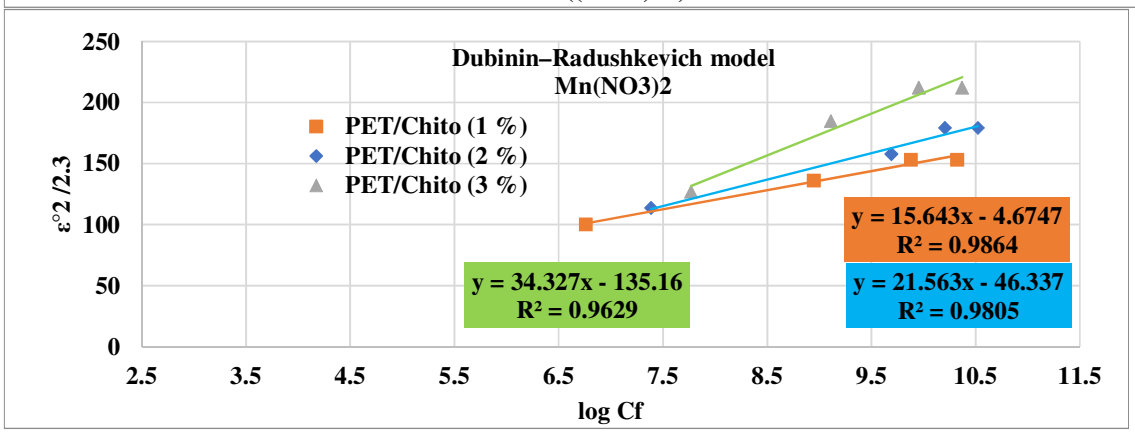

Figure 13: Isothermal models for **$Mn(NO_3)_2$**using different used nanofibres

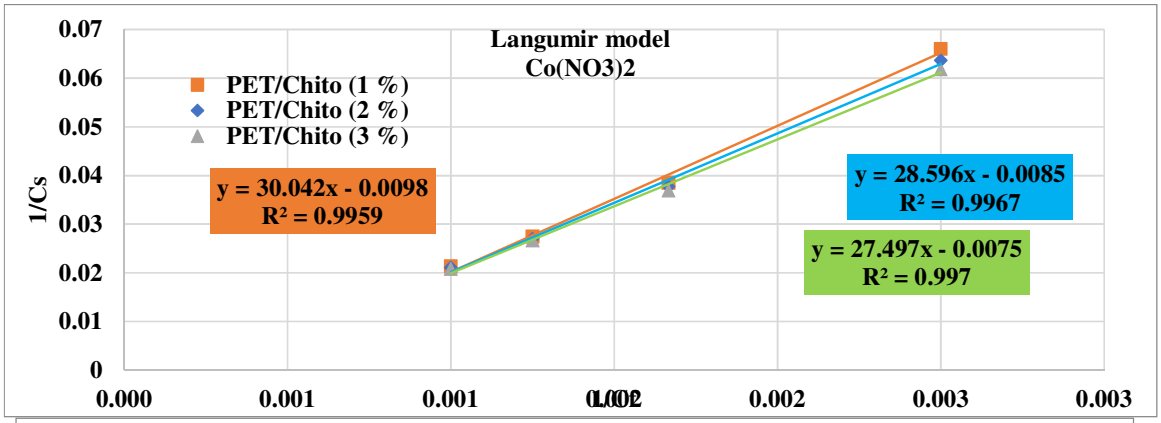

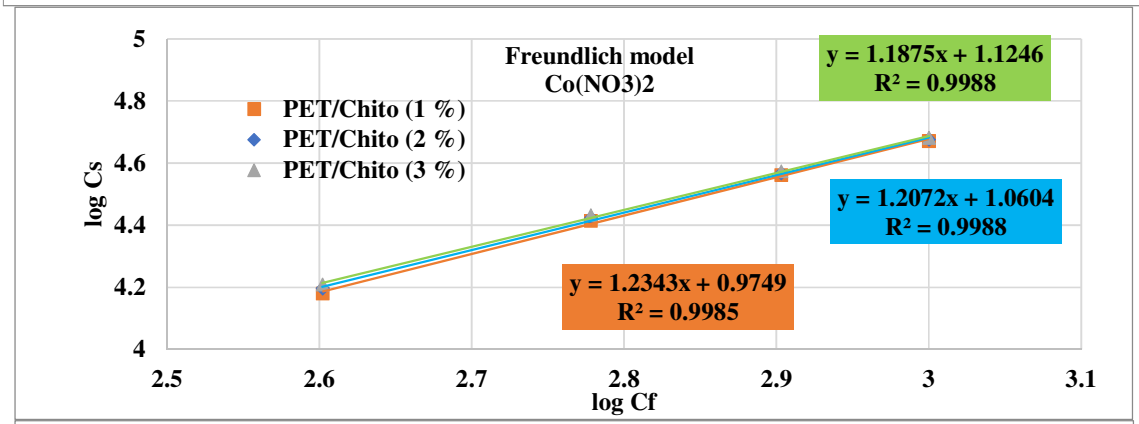

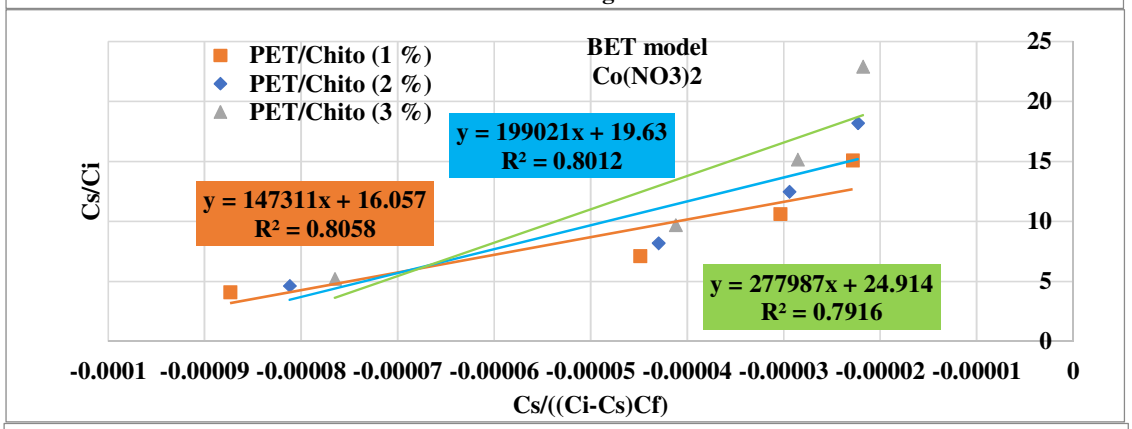

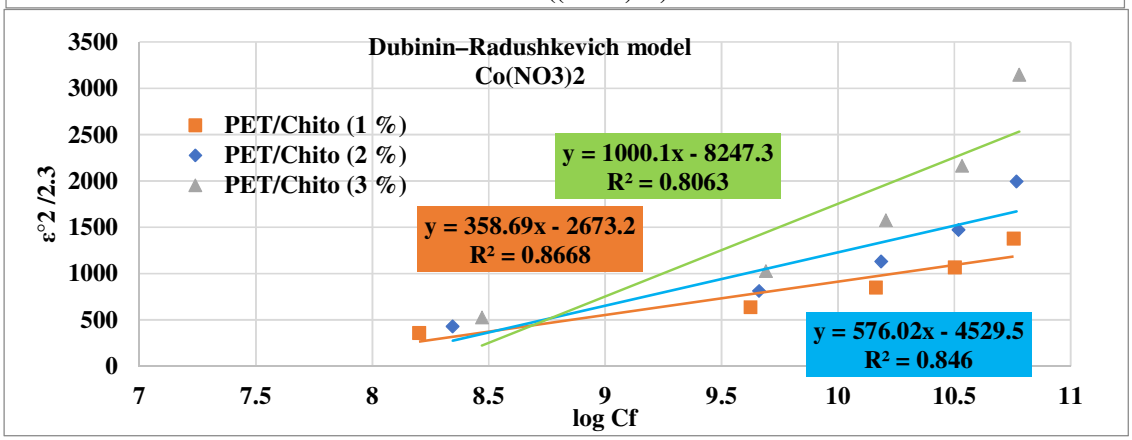

Figure 14: Isothermal models for $Co(NO_3)_2$using different used nanofibres

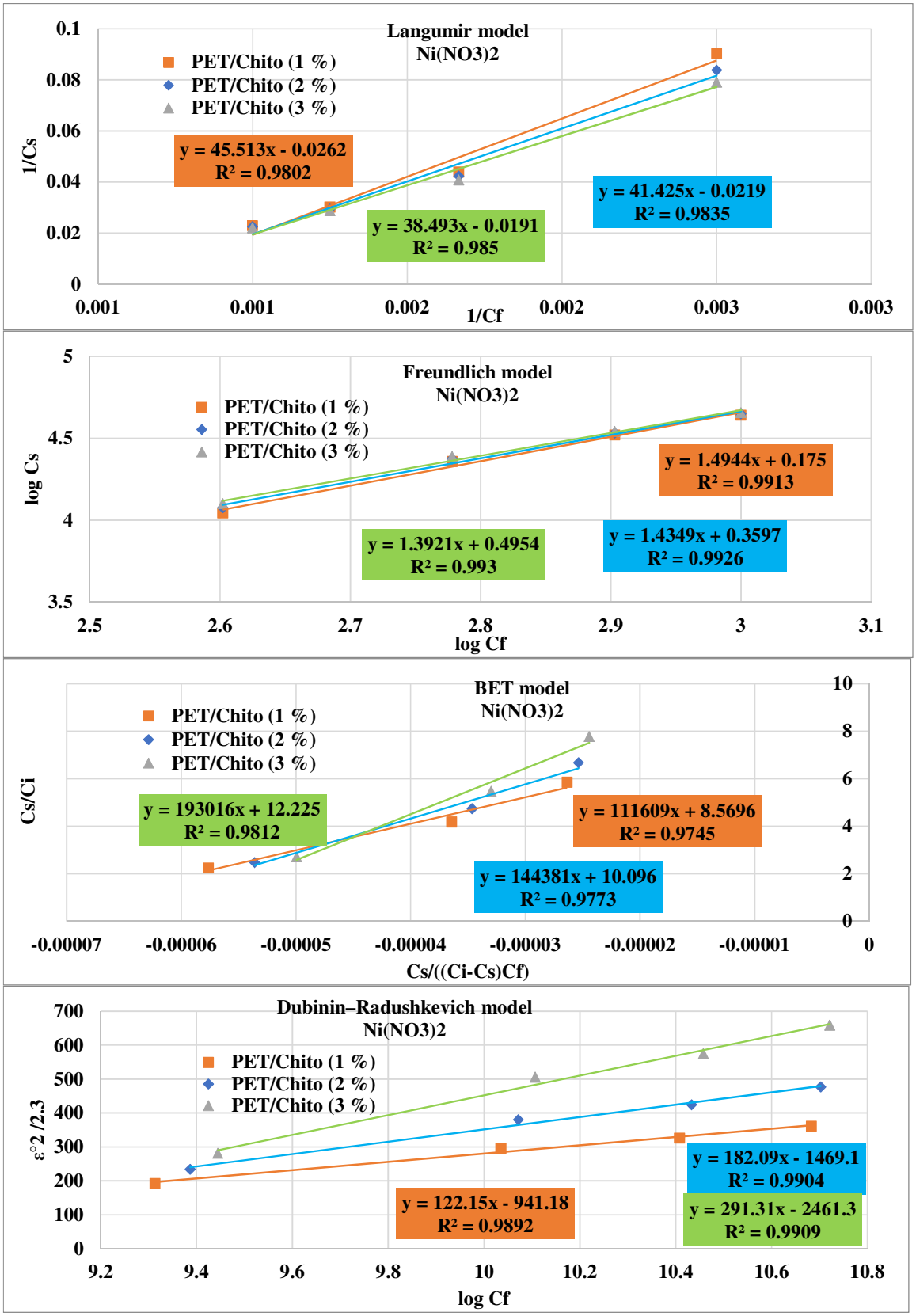

Figure 15: Isothermal models for $Ni(NO_3)_2$using different used nanofibres

Table 4: Comparison between the parameters of adsorption isotherm models for various metal salts on three different nanofibres with chitosan

Nanofiber	Parameters	Isothermal Models															
		Ba^{+2}				Mn^{+2}				Co^{+2}				Ni^{+2}			
		Langmuir	Freundlich	BET	D – R	Langmuir	Freundlich	BET	D – R	Langmuir	Freundlich	BET	D – R	Langmuir	Freundlich	BET	D – R
PET/Chito 1 %	R^2	0.9930	**0.9974**	0.8446	0.9955	0.9592	**0.9808**	0.7559	0.9717	0.9959	**0.9985**	0.8058	0.9340	0.9802	**0.9913**	0.8004	0.9892
	C_{max}(mg/g)	-7.278	45.146	0.002	0	-1.8069	40.04	0.011455	1.0000	-10.165	46.874	0.001	0	-3.815	43.612	0.003	0
	K	-249.459	5.711	5747.291		-129.704	0.1615	1964.024		-305.36	9.437	9175.423		-173.645	1.496	4522.713	
	1/n		1.302				1.81059				1.234				1.494		
	β				-128.838				-6.42E-06				-625.09				-122.15
	E				0.06				0.09				0.03				0.06
	RMSE	44.883	33.496	36.645	36.646	33.376	32.117	31.449	30.426	50.184	33.783	38.456	38.457	38.986	34.105	34.838	34.841
	X^2	-830.364	74.557	2668678		-1853.00	157.364	259012.6	2779.352	-743.30	73.045	6536423		-1195.14	80.011	1209160	
	SAE	112.395	254.571	61.444	61.448	116.471	176.441	103.788	100.822	116.511	282.758	45.357	45.359	105.402	226.587	78.686	78.695
	ARE	160.303	274.059	99.987	100.000	108.797	94.916	99.944	95.132	218.212	445.135	99.992	100.000	124.891	184.527	99.980	100.000
PET/Chito 2 %	R^2	0.9969	**0.9988**	0.8667	0.9961	0.9969	**0.9988**	0.8240	0.9323	0.9967	**0.9988**	0.8012	0.9210	0.9835	**0.9926**	0.8114	0.9904
	C_{max}(mg/g)	-13.942	47.654	0.000	0.000	-13.942	47.654	0.004	6.9E-219	-11.786	47.438	0.001	0.000	-4.558	44.458	0.002	0.000
	K	-381.162	14.211	10271.18		-381.162	14.211	4877.371		-337.01	11.492	10139.73		-188.797	2.289	5381.735	
	1/n		1.177				1.177				1.207				1.435		
	β				-778.751				-64.018				-1015.22				-182.09
	E				0.06				0.09				0.02				0.06
	RMSE	52.766	36.179	36.646	36.646	47.219	40.550	31.457	31.4609	52.116	34.378	38.456	38.457	39.813	34.998	34.839	34.841
	X^2	-599.092	82.401	8305303		-479.751	103.516	773553.3	4.2E+221	-691.37	74.740	8830830		-1043.37	82.653	1692583	
	SAE	159.044	272.128	61.447	61.448	201.418	229.754	103.811	103.822	127.857	286.708	45.357	45.359	110.598	232.512	78.689	78.695
	ARE	215.520	294.840	99.996	100.000	167.875	131.994	99.981	100	237.064	451.697	99.994	100.000	129.734	190.048	99.986	100.000
PET/Chito **3 %**	R^2	0.9779	**0.9924**	0.6301	0.8026	0.9677	**0.9843**	0.7823	0.9680	0.9970	**0.9988**	0.7916	0.9100	0.9850	**0.9930**	0.8195	0.9909
	C_{max}(mg/g)	-2.948	45.388	0.0029	0.000	-2.445	41.542	0.0064	2.0E+149	-13.246	48.002	0.00035	0.000	-5.245	45.304	0.0015	0.000
	K	-151.924	0.610	4242.816		-143.603	0.438	2861.989		-364.23	13.323	11158.71		-201.904	3.129	5241.008	
	1/n		1.630				1.669				1.187				1.392		
	β				-149.346				14.8042				-1000.07				-130.82
	E				0.06				0.8				0.02				0.06
	RMSE	39.921	33.751	36.643	36.646	34.064	33.723	31.454	2.6E+149	53.867	34.978	38.457	38.457	40.585	35.902	34.839	34.841
	X^2	-1621.74	75.293	1388376		-1423.564	82.126	459436.2	1.0E+150	-657.16	76.462	1233467		-942.071	85.354	2350620	
	SAE	82.085	256.270	61.440	61.448	120.940	186.974	103.803	1.4E+150	138.082	290.658	45.357	45.359	115.411	238.436	78.690	78.695
	ARE	124.427	276.070	99.976	100.000	111.905	102.242	99.969	9.9E+149	254.051	458.259	99.996	100.000	134.220	195.570	99.990	100.000

4. Conclusion

The study investigated the adsorption properties of PET/Chitosan nanofibers for various heavy metal salts, including $Ba(NO_3)_2$, $Mn(NO_3)_2$, $Co(NO_3)_2$, and $Ni(NO_3)_2$. The key findings are:

- Adsorption kinetics: The pseudo-second-order kinetics model provided the best fit for the adsorption data, indicating a diffusional mechanism through micropores. However, intraparticle diffusion was not the sole rate-limiting step, suggesting multiple kinetic processes contribute to the sorption mechanism.
- Adsorption efficiency: As the chitosan content in the nanofibers increased from 1% to 3%, the maximum adsorbed heavy metal salt concentration increased. However, the adsorption efficiency decreased with increasing heavy metal salt concentration, particularly beyond 400 mg/L.
- Isotherm models: The Freundlich adsorption model showed the best alignment with experimental data, suggesting multilayer coverage of heavy metal salts on the PET/Chitosan nanofibers. The n values from the Freundlich model were less than 1, indicating favorable chemical adsorption.
- Adsorption mechanism: The Dubinin-Radushkevich model revealed that the adsorption process was chemisorption, with mean free energy (E) values increasing with chitosan content in the nanofibers.
- Comparison with other adsorbents: The PET/Chitosan nanofibers demonstrated competitive adsorption capacities compared to other non-conventional adsorbents reported in the literature.

In conclusion, PET/Chitosan nanofibers show promise as effective adsorbents for heavy metal salt removal from aqueous solutions. The adsorption process is characterized by chemical interactions, multilayer coverage, and diffusion through micropores. These findings suggest that PET/Chitosan nanofibers could be valuable in environmental remediation and water treatment applications, particularly for the removal of heavy metal contaminants.

5. Conflict of interest

The authors declare that there is no conflict of interest.

6. Declaration section

The datasets used and/or analyzed during the current study are available from the corresponding author upon reasonable request.

7. Acknowledgments

The authors are gratefully grateful to acknowledge the Ain Shams University, Faculty of Graduate Studies and Environmental Research Basic Science Department, Cairo, Egypt. Furthermore, the authors are gratefully grateful to acknowledge the Chemical Engineering Department, National Research Centre Higher Institute of Engineering, El-

Shorouk Academy, Cairo, Egypt. Furthermore, the authors are gratefully grateful to acknowledge the Central Labs Services (CLS) and Centre of Excellence for Innovative Textiles Technology (CEITT) in Textile Research and Technology Institute (TRTI), National Research Centre (NRC) for the facilities provided.

8. Reference

[1]. A.J. Echendu, H.F. Okafor, O. Iyiola, Air pollution, climate change and ecosystem health in the niger delta, Social Sciences 11(11) (2022) 525.
[2]. S.S. Shetty, S. Sonkusare, P.B. Naik, H. Madhyastha, Environmental pollutants and their effects on human health, Heliyon (2023).
[3]. N. Sharma, B.J. Allardyce, R. Rajkhowa, R. Agrawal, Rice straw-derived cellulose: A comparative study of various pre-treatment technologies and its conversion to nanofibres, Scientific Reports 13(1) (2023) 16327.
[4]. B. Nasri-Nasrabadi, T. Behzad, R. Bagheri, Extraction and characterization of rice straw cellulose nanofibers by an optimized chemomechanical method, Journal of Applied Polymer Science 131(7) (2014).
[5]. M.M. El-Zawahry, F. Abdelghaffar, R.A. Abdelghaffar, A.G. Hassabo, Equilibrium and kinetic models on the adsorption of reactive black 5 from aqueous solution using eichhornia crassipes/chitosan composite, Carbohydrate Polymers 136 (2016) 507-515.
[6]. A.G. Hassabo, A.L. Mohamed, Multiamine modified chitosan for removal metal ions from their aqueous solution BioTechnology: An Indian Journal 12(2) (2016) 59-69.
[7]. E. El-Sayed, H.A. Othman, A.G. Hassabo, Cyclodextrin usage in textile industry, J. Text. Color. Polym. Sci. 18(2) (2021) 111-119.
[8]. A.G. Hassabo, M. Zayed, M. Bakr, E. Abd El-Aziz, H. Othman, Applications of supercritical carbon dioxide in textile finishing: A review, J. Text. Color. Polym. Sci. 19(2) (2022) 179-187.
[9]. E. Abd El-Aziz, R.H. Abd El-Rahman, A.A. Mokhtar, S.S. El-Desoky, G.A. El-Bahrawy, H.A. Ezat, A.G. Hassabo, Textile effluent as a potential problem for environmental and human health: Causes and overcome techniques, Egy. J. Chem. 66(12) (2023) 445 - 453.
[10].M.M. El-Zawahry, A.G. Hassabo, A.L. Mohamed, Preparation of cellulose gel extracted from rice straw and its application for metal ion removal from aqueous solutions, Int. J. Biol. Macromol. 248 (2023) 125940.
[11].S.A. Ebrahim, H. Othman, A.G. Hassabo, Enhancing polymer matrix reinforcements: Exploring the potential of biologically modified clay minerals in dyeing, pigment dyes, and wastewater treatment, J. Text. Color. Polym. Sci. (2024) -.
[12].L.S. Abd-Elaal, A.N. El-Wekil, A.G. Marey, L.N. Allam, A.G. Hassabo, Supercritical carbon dioxide as an impregnation medium for producing functional materials in textile finishing, J. Text. Color. Polym. Sci. 22(1) (2025) 187-195.
[13].M.M. El-Zawahry, A.G. Hassabo, F. Abdelghaffar, R.A. Abdelghaffar, O.A. Hakeim, Preparation and use of aqueous solutions magnetic chitosan / nanocellulose aerogels for the sorption of reactive black 5, Biointerf. Res. Appl. Chem. 11(4) (2021) 12380 - 12402.
[14].M.I. Muhib, M.K. Uddin, M.M. Rahman, G. Malafaia, Occurrence of microplastics in tap and bottled water, and food packaging: A narrative review on current knowledge, Science of The Total Environment 865 (2023) 161274.
[15].M.A. Fayshal, Current practices of plastic waste management, environmental impacts, and potential alternatives for reducing pollution and improving management, Heliyon 10(23) (2024).
[16].X. Li, Y. Peng, Y. Deng, F. Ye, C. Zhang, X. Hu, Y. Liu, D. Zhang, Recycling and reutilizing polymer waste via electrospun micro/nanofibers: A review, Nanomaterials 12(10) (2022) 1663.
[17].F. Awaja, D. Pavel, Recycling of pet, Eur. Polym. J. 41(7) (2005) 1453-1477.
[18].AATCC Test Method (195-2011e2(2017)e3), Test method for liquid moisture managementproperties of textile fabrics, Technical Manual Method American Association of Textile Chemists and Colorists, 2021, p. 398.
[19].M.N. Sahmoune, K. Louhab, Kinetic analysis of trivalent chromium biosorption by dead streptomyces rimosus biomass, The Arabian Journal for Science and Engineering 35(2B) (2010) 69-80.
[20].M.N. Sahmoune, K. Louhab, A. Boukhiar, Biosorption of cr (iii) from aqueous solutions using bacterium biomass streptomyces rimosus, International Journal of Environmental Research 3(2) (2009) 229-238.
[21].K.L. Wasewar, M. Atif, B. Prasad, I.M. Mishra, Adsorption of zinc using tea factory waste: Kinetics, equilibrium and thermodynamics, CLEAN – Soil, Air, Water 36(3) (2008) 320-329.
[22].H. Liu, Y.L. Hsieh, Ultrafine fibrous cellulose membranes from electrospinning of cellulose acetate, Journal of Polymer Science Part B: Polymer Physics 40(18) (2002) 2119-2129.
[23].H. Othman, E.A. Awad, S.A. Zaher, L.T. Mohamed, E.A. Dabour, E.S. Youssif, M.A. Almouregi, A.G. Hassabo, Electrospinning process parameters and application: A review, J. Text. Color. Polym. Sci. 22(1) (2025) 59-66.
[24].A.L. Mohamed, A.G. Hassabo, A.A. Nada, S. Zaghlool, Encapsulation of nicotinamide into cellulose based electrospun fibres, JAPS 6(8) (2016) 13-21.
[25].A.A. Nada, R.A. Abd El-Azeem, A.G. Hassabo, A.L. Mohamed, H.M. Ibrahim, W. Fayad, N.Y. Abou-Zeid, Encapsulation of ricinoleic acid into electrospun ethyl cellulose fibers, 11th International Conference on Nanosciences & Nanotechnologies – NN14, Porto Palace Conference Centre & Hotel, Thessaloniki, Greece, 2014.
[26].A.G. Hassabo, A.L. Mohamed, T.A. Khattab, Preparation of cellulose-based electrospun fluorescent nanofibres doped with perylene encapsulated in silica nanoparticles for potential flexible electronics, Luminescence 37(1) (2022) 21-27.
[27].M. Rehan, S. Zaghloul, F.A. Mahmoud, A.S. Montaser, A. Hebeish, Design of multi-functional cotton gauze with antimicrobial and drug delivery properties, Materials Science and Engineering: C 80 (2017) 29-37.
[28].M.M. Abd El-Hady, A. Farouk, S.E.-S. Saeed, S. Zaghloul, Antibacterial and UV protection properties of modified cotton fabric using a curcumin/TiO2 nanocomposite for medical textile applications, Polymers 13(22) (2021) 4027.

[29].H.E. Emam, S. Zaghloul, H.B. Ahmed, Full ultraviolet shielding potency of highly durable cotton via self- implantation of palladium nanoclusters, Cellulose 29(8) (2022) 4787-4804.
[30].E.M. Reda, H.A. Othman, H. Ghazal, A.G. Hassabo, Kinetic and isothermal study of dye absorption using pre-treated natural fabrics using polyamine compounds, Scientific Reports 15(1) (2025) Article number: 3794.
[31].M. Er-Rafik, A.L. Mohamed, M. Möller, K. Spyropoulos, R. Wagner, Advanced textile enhancers- magnasoft silq®: Investigation of the deposition onto cotton fibers, Melliand Inter. 5(47-54) (2012) 3157.
[32].A.G. Hassabo, A. Mendrek, C. Popescu, H. Keul, M. Möller, Deposition of functionalized polyethylenimine-dye onto cotton and wool fibres, RJTA 18(1) (2014) 36-49.
[33].A.L. Mohamed, A.G. Hassabo, Engineered carbohydrate based material/silane as a thermo and pH-sensitive nanogel containing zinc oxide nanoparticles for antibacterial textile, International Conference on Medical Textiles and Healthcare Products (MedTex 2015), Department of Material and Commodity Sciences and Textile Metrology, Faculty of Material Technologies and Textile Design, Lodz University of Technology, Lodz, Poland, 2015.
[34].H.E. Emam, A.L. Mohamed, Controllable release of povidone-iodine from networked pectin@carboxymethyl pullulan hydrogel, Polymers 13 (2021) 3118(1-21).
[35].N. Kannan, M.M. Sundaram, Kinetics and mechanism of removal of methylene blue by adsorption on various carbons--a comparative study, Dyes Pigm. 51(1) (2001) 25-40.
[36].Y.S. Ho, D.A.J. Wase, C.F. Forster, Kinetic studies of competitive heavy metal adsorption by sphagnum moss peat, Environmental Technology 17(1) (1996) 71-77.
[37].X. Xu, B.-Y. Gao, Q.-Y. Yue, Q.-Q. Zhong, Preparation and utilization of wheat straw bearing amine groups for the sorption of acid and reactive dyes from aqueous solutions, Journal of Hazardous Materials 182(1–3) (2010) 1-9.
[38].A.G. Hassabo, Synthesis and deposition of functional nano-materials on natural fibres RWTH Aachen University, Germany, 2011, p. 154.
[39].S. Wang, Y. Boyjoo, A. Choueib, Z.H. Zhu, Removal of dyes from aqueous solution using fly ash and red mud, Water Res. 39(1) (2005) 129-138.
[40].F. Doulati Ardejani, K. Badii, N. Yousefi Limaee, S.Z. Shafaei, A.R. Mirhabibi, Adsorption of direct red 80 dye from aqueous solution onto almond shells: Effect of pH, initial concentration and shell type, Journal of Hazurdous Materials 151(2-3) (2008) 730 - 737.
[41].A.O. Dada, A.P. Olalekan, A.M. Olatunya, O. DADA, Langmuir, freundlich, temkin and dubinin-radushkevich isotherms studies of equilibrium sorption of zn2+ unto phosphoric acid modified rice husk, Journal of Applied Chemistry 3(1) (2012) 38-45.
[42].B.H. Hameed, D.K. Mahmoud, A.L. Ahmad, Equilibrium modeling and kinetic studies on the adsorption of basic dye by a low-cost adsorbent: Coconut (cocos nucifera) bunch waste, Journal of Hazardous Materials 158(1) (2008) 65-72.
[43].S. Sahoo, Uma, S. Banerjee, Y.C. Sharma, Application of natural clay as a potential adsorbent for the removal of a toxic dye from aqueous solutions, Desalination and Water Treatment 52(34-36) (2014) 6703-6711.
[44].A.L. Mohamed, A.G. Hassabo, S. Shaarawy, A. Hebeish, Benign development of cotton with antibacterial activity and metal sorpability through introduction amino triazole moieties and agnps in cotton structure pre-treated with periodate, Carbohydrate Polymers 178 (2017) 251-259.
[45].M.M. El-Zawahry, M.M. Kamel, A.G. Hassabo, Development of bio-active cotton fabric coated with betalain extract as encapsulating agent for active packaging textiles, Indust. Crop. Prod. 222 (2024) 119583.